Responses to Referees' Comments on "S2P3-R (v1.0): a framework for efficient regional modelling of physical and biological structures and processes in shelf seas" (revised) by R. Marsh et al. (gmd-2014-256)

Overview of Responses

We thank the referees for further extensive and informative comments. Below, we list these verbatim (italic text), responding to each comment in turn. In the revised manuscript, the revised text is highlighted in red.

Response to Referee #1

Line no:

20: Comma use (projects,) makes the sentence unwieldy with a clause and introductory part. This could be separated into two sentences to make it easier to read.

Response: We have split the text as follows, "In such cases, S2P3-R may be used as a highly versatile research tool, alongside more complex and computationally expensive models. In undergraduate oceanography modules and research projects, the model serves as an effective practical tool for linking theory and field observations." (lines 24-27).

22: evaluated twice.

Response: We have removed the first occurrence of "evaluated".

27: I am assuming that an American dictionary is being used, seeing as the majority of spelling is in this form. However, there are a few UK spellings in here as well. For example, search for analyse.

Response: We have checked spelling - "emphasized" is changed to "emphasised" (lines 33, 88, 280).

34: A lot of the operational applications I am aware of use the required resolution to address certain questions or aspects of the marine system. This sentence makes it sound like resolution is increased to reflect technical ability alone. I don't agree with this.

Response: We have simplified the statement and removed a redundant sentence, so the relevant text now reads, "A variety of models have been developed to explore the processes that shape and maintain productivity. Operational biogeochemistry and ecosystem models typically represent the system with relatively high complexity and resolution, e.g., the 7 km Atlantic Margin Model NEMO-ERSEM (AMM7-NE) system (Edwards et al., 2012)" (lines 37-41).

42: use commas in reference here and not elsewhere.

Response: Corrected throughout

45: Split the sentence to aid readability. "Central to the model physics… NP) model" and then the efficiency of the seasonal cycle can be included in the following sentence after "In this way"

Response: We have split the text, as follows, "Central to the model physics is a turbulence closure scheme, determining the light environment and nutrient fluxes that drive a simple

primary production (nutrient-phytoplankton, or NP) model. Phytoplankton growth responds to changes in stratification and mixing." (lines 50-53).

85: break,

Comma added

129: (T)

T bracketed

249: Split "Default mapped.." sentence

Response: We have split the text as follows, "Default mapped variables are the mid-summer surface-bottom temperature difference, annual-mean surface heat flux, and annual net production. Other quantities, such as the mid-summer sub-surface chl-a maximum (SCM) and SCM depth, can also be mapped." (lines 252-255).

312: Analyse: Proper English spelling :o)

386: I realise it is probably more the case of how you view the forcing files but I don't understand how artefacts can be added to the forcing from reading this text.

Response: We have re-structured the paragraph to explain more clearly, "We have also experimented, on the northwest European shelf domain, with spatially discriminate initial temperatures and meteorological forcing (not shown here), the latter respecting variation of NCEP reanalysis data (per 2.5° grid square) across the domain. While this approach has the potential to restrict net heat fluxes closer to zero at all locations, coarse-resolution data must be carefully interpolated to the relatively fine 12-km mesh of S2P3-R in order to avoid unrealistic horizontal variations in forcing and simulated fields." (lines 385-391).

419: split sentence

Response: We have split the text as follows, "The model does not reproduce the enhanced primary production and chl-a observed in the surface at the Celtic Sea shelf break (e.g., compare Figs. S4 and S5, for April and May). This is likely because it does not include specific physical processes, such as the internal tide, that are important for vertical nutrient supply to the surface in these regions (Sharples et al., 2007)." (lines 423-427).

625: You assume that vertical processes are more important than lateral, non-tidal, ones. However, reading the text I would argue that you're a-priori assumption here is not valid for the domain you intend to model. I do not think the model system you propose is flawed but a more important and fundamental question concerns what the model structure lacks. As this is a GMD paper, I agree that this model should be published. However, if you propose to essentially expand the capability of SPR3-R to accommodate horizontal processes, the obvious question has to be why? There are probably much more appropriate model structures to accommodate fresh water inputs for example. A comparison with a NEMO-NPZD or a NEMO-ERSEM (as this seems to be the forerunner at present) could result in a study showing how well the models perform (as far as I am aware NEMO-ERSEM has not been proven to work well in domain influenced by fresh-water inputs). Of importance is an identification of what needs to be included in the next model descriptions to address relevant questions and in particular simulate conditions in particular domains. The more fine scale, land-ocean, interaction model simulations I have in mind are so for specific reasons.

Response: We agree with the reviewer that further development of S2P3-R to implicitly include horizontal processes may not be appropriate. With this in mind, we have subtly re-phrased the relevant sentence as follows, "The realism of S2P3-R depends on the extent to which vertical processes dominate horizontal processes. This is evident across some shelf sea regions, where we have the high-quality observations necessary for a co-evaluation of these processes." (lines 628-630). We have also removed, from Section 4, the three points (previously lines 679-686) specific to this development, and corresponding text in the closing paragraph of Sect. 1 (line 89).

646: ease? I don't think the ease with which something can be implemented should feature in this discussion. If a model is not able to do a job, it should not be used.

Response: We have removed this clause, so the sentence now reads, "Our simpler approach thus indicates the importance of 1-D processes in forming these features, the locations of which are consistent with these more complex (hence expensive) models." (lines 656-657).

997: Figure 8

Corrected.

Response to Referee #2

Re-review of "S2P3-R(v1.0): a framework for efficient regional modeling of physical and biological structures and processes in shelf seas" by Marsh, Hickman and Sharples.

The authors have done a nice job with their edits of the manuscript, which has been considerably improved. In particular, I feel that their final paragraph is an excellent summary of the modeling framework they are presenting. However I still have issues with a few of the authors' points, which do need further attention.

(1) On lines 69-72 the authors state in the revised manuscript: "S2P3 has not been extensively used and tested across real transects or in regions where 1D (vertical) processes are dominant, such that the model can be appropriately used for investigating time evolving 3D structures." In my opinion, it is misleading to imply that S2P3-R can be used to investigate time-evolving 3D structures. As I understand it, the modeling framework essentially involves running many many model implementations in 1D at sites that are ~1 km apart. Thus S2P3 can help us understand how vertical processes vary in the horizontal, but this is fundamentally different from helping us understand 3D processes. The authors do say "3D structures" and not "3D processes", but I feel it is likely that this point will be misinterpreted by readers. Thus I feel the authors need to make it clearer to the reader that this modeling framework: (1) does not provide a tool to examine 3D processes, but rather provides a tool to look at how vertical processes vary in horizontal space and (2) should only be used in regions where horizontal processes (such as horizontal advection) are known to be weak. Both of these points must be added to the abstract.

Response: Following the reviewer's advice, we have added the following sentences to the Abstract, "While not representing 3-D processes, S2P3-R reveals the horizontal variation of the key 1-D (vertical) processes. S2P3-R should therefore only be used in regions where horizontal processes - including mean flows, eddy fluxes and internal tides - are known to exert a weak influence in comparison with vertical processes." (lines 20-24).

(2) It would be very helpful for readers and potential future users of the framework if the authors could recommend quantitative methods for determining if a region is characterized by weak horizontal advection, and thus suitable for this modeling framework. For example, the authors state: "1D (vertical) processes dominate 2D (horizontal) processes across much

3

of the shelf seas, where we have the observations necessary for a co-evaluation of these processes." I feel that this is an important component of the manuscript, and that this quantitative co-evaluation of vertical vs. horizontal processes should be included in the manuscript.

Response: Introducing a quantitative method for such an evaluation would be a major undertaking, and the very short timescale for minor revisions (10 days) and we are unable to develop this aspect of the framework at such short notice. However, in Sect. 4, we propose one such method, with the following text, "One way to formally quantify the dominance of surface net heat fluxes and tidal plus wind mixing (the 1-D processes) is by calculating tendencies of the potential energy anomaly (PEA, see Chapter 6 in Simpson and Sharples, 2012). PEA tendencies calculated directly from observed changes of stratification at selected locations (e.g., weekly/monthly at Western Channel Observatory stations L4/E1) can be compared with indirect estimates computed from time-integrated heat fluxes, winds and tidal currents at the same locations. If local heat fluxes and tidal/wind mixing dominate the annual cycle of stratification, directly calculated and indirectly estimated time series of PEA tendency should be similar." (lines 630-639).

(3) I disagree with the statement that "the 1D approach is however valid for testing, against suitable observations of evolving physical structures, the extent to which advection may be important"(lines 696-698). Just as the authors state in their response document, the model-data discrepancy in Fig. 4 could be due to the missing horizontal processes, or it could be due to the relatively simple description of phytoplankton physiology. A 1D model framework cannot be used to determine the importance of horizontal processes simply be assessing model-data mismatch. There are multiple other potential explanations for model-data mismatch.

Response: We have removed the entire paragraph (as requested below), as all other points are repeated above and below in Sect. 4.

(4) I recommend removing almost all usage of "3D" within the manuscript, except where the authors are stating that this is not a 3D model. The overuse of "3D" makes it seem to the reader as if 3D processes are being modeled, but of course they are not. Similarly "2D" should be removed and replaced with "horizontal" to avoid unnecessary confusion. (In many situations "2D" represents x-z variability, not x-y variability.)

Response: Done

Specific comments:

Abstract – Change line 15-16 to: "...can be efficiently used to study the horizontal variability of vertical processes in shelf seas or other regions where horizontal advection is negligible, such as in the tidal mixing fronts that develop…"

Response: We have expended the text in this part of the Abstract as follows, "This Regional adaptation of S2P3, the S2P3-R framework (v1.0), can be efficiently used to investigate physical and biological phenomena in shelf seas that are strongly controlled by vertical processes. These include spring blooms that follow the onset of stratification, tidal mixing fronts that seasonally develop at boundaries between mixed and stratified water, and sub-surface chlorophyll maxima that persist throughout summer." (lines 15-20). See also our response to Referee #1.

Line 52 – word missing (to?)

Response: Corrected - thank you for spotting this!

Line 70-71 – this sounds as if S2P3 has been extensively used in regions where 1D vertical processes are not dominant? I'm not sure this is what the authors intend to say here, but if it is, references are needed.

Response: We have modified this sentence as, "In spite of potential for widespread application, S2P3 has not been extensively used and tested across real transects or in limited regions, where the model can be appropriately used for investigating time-evolving stratification and biological productivity." (lines 74-77).

Line 72 – change to "used for investigating the horizontal variability of 1D structures"

Response: In response to an earlier comment, this is changed to "… used for investigating time-evolving stratification and biological productivity" (lines 76-77).

Line 73 – simply remove "3D" or change to "to efficiently model the horizontal variability of physical and biological structures in shelf seas"

Response: We removed "3D".

Line 75 – change to "facilitated the simulation of vertical processes and their horizontal variability in real-time…"

Response: Done.

Line 465 – if the model overestimates the observations by a factor of two at most depths as stated in the text, I disagree with the statement that "the model reproduces the observations".

Response: We have revised the sentence opening accordingly, as "Comparing the simulation with the observations, …" (line 469).

Line 622 – should be "complement".

Response: Corrected - thank you for spotting this!

Line 626 – remove 1D and 2D and parentheses

Response: Done.

Line 635 – replace "unprecedented" with "high". Some coupled 3D biological-physical models are run in estuaries and continental shelves (e.g. FVCOM) at resolution as high as a few hundreds of meters. Physical models are routinely run at resolutions as high as 50m (http://www.sciencedirect.com/science/article/pii/S007966111400130X) The horizontal resolution used here is not unprecedented in terms of 3D modeling.

Response: We choose the terminology "appropriately high" (line 647).

Line 637 – remove "3D"

Response: Done.

Line 645 – remove "(hence expensive)". Evidence of this is not provided. If a 3D model is already set up and running, it would actually be more expensive to develop a new 1D model framework.

Response: Done.

Line 653 – again, this resolution is not unprecedented.

Response: Here we now refer to "very high horizontal resolution" (line 664).

Line 654 – but if massively parallel computing resources were available, why not actually run a 3D model that includes horizontal processes? Even if it takes a week to run instead of a few minutes, in terms of the total amount of time it takes to complete a research project, the run-time of a high resolution 3D model is typically quite small. The true benefit of this framework is that it can be used by those who do not have access to, or the knowledge of how to use, parallel computing resources.

Response: Fair point. We have removed the sentence "Massively parallel computing would of course reduce compute time by several orders of magnitude."

Line 657 – what is meant by "temperature structures"? The word structure is used frequently throughout the manuscript, but it is a rather confusing terminology. Replace "3D temperature structures" with "Temperature distributions"

Response: In most places, we have changed the terminology accordingly. In a few cases, we consider the use of "structures" appropriate, notably in the title, where we specify "physical and biological structures".

Line 697 – I disagree, as noted above. Please remove this paragraph.

Done.

Line 700-708 – very nice final paragraph!

Thank you!

Response to Additional Report of Referee #3

I have read the paper and the author's responses to the reviewers' initial comments. My conclusion is that I agree with the reviewer who stated that "although the manuscript is well written, I feel that the content is more suitable for a technical report appearing on a modeling website, than a peer-reviewed publication in GMD." The manuscript seems to be an account of what an already-described model can do, but contains no clear research questions and thus no significant new information.

I also agree with the reviewer's comment that "the authors are essentially attempting to study 3D physical/biological shelf processes by ignoring advection. In many/ most shelf systems, advective processes play a critical role in controlling the distributions of nutrients and phytoplankton." Although I have used (and published) accounts of 1-D (z-t) models, and argued for the importance of 'vertical processes' in the short-term control of phytoplankton dynamics, I don't think it is possible to make reliable maps of biogeochemical processes in shelf seas using a grid of 1D models and without taking account of salinity. A specific concern is with the effect of lateral transports of freshwater buoyancy and nutrients, which are important in parts of the greater North and Celtic Seas, and I guess to be important in the east China Sea (e.g. the Chiangjiang plume).

Thus there is a scientific as well as a structural ground for recommending rejection. To end on a positive note, and to encourage the use of the S2P3 model in appropriate circumstances,

the authors might consider publishing maps showing (e.g. for the NE European shelf) the magnitude of discrepancies between observed and simulated variables.

The referee largely reiterates comments of Referees #1 and #2, to which we have responded at length in two rounds of revision. However, we take the opportunity to respond to some specific points made above.

It is not necessary for a GMD model evaluation manuscript to pose "research questions" as such, although we have made clear in Sect. 4 that S2P3-R can be used "… to test hypotheses regarding the sensitivity of 1-D biogeochemical processes to key model parameters, and/or to test the responses to variations of physical forcing on timescales ranging from diurnal to interannual." (lines 696-698).

Regarding the perception that we are ignoring horizontal processes, it should now be clear that the necessary caveats are clearly stated, e.g., in the Abstract, "While not representing 3-D processes, S2P3-R reveals the horizontal variation of the key 1-D (vertical) processes. S2P3-R should therefore only be used in regions where horizontal processes - including mean flows, eddy fluxes and internal tides - are known to exert a weak influence in comparison with vertical processes." (lines 20-24).

Regarding the importance of neglecting variable salinity, and associated forcing, this is only likely to dominate buoyancy forcing (over the surface heat flux) near points of high runoff (i.e., near coasts and major rivers), and we no longer plan to admit horizontal processes indirectly (see response to Referee #1). We now emphasise the use of S2P3-R away from coastal influences, where temperature is by far the dominant control on density and stratification, supported by the successful mapping of tidal mixing fronts around the UK (see Fig. 3a,b).

The close correspondence between observed and simulated stratification at E1 suggests that vertical processes, specifically the surface net heat flux and wind/tidal mixing, likely dominate across those limited regions for which stations such as E1 are representative, and in Sect. 4 we now propose a means for quantifying this via the potential energy anomaly (lines 630-639). Admittedly, S2P3-R is designed for use away from coasts and open ocean boundaries, where horizontal processes are important, and this is clearly recognised in Sect. 4 (lines 678-687).

Regarding the use of S2P3-R to map variables for comparison with observations (to more clearly indicate where the model is valid), this is indeed an aspiration, although in the absence of fine-resolution sub-surface variables, we may have to compare our simulations with those obtained using dynamical models such as the NEMO-ERSEM (AMM7-NE) system. Our comparison of simulated and observed *surface* chl-a concentrations suggests considerable scope for improvement via tuning of key parameters. In the case of the European shelf, we modified a statement in Sect. 3.1 to reflect this, "The model broadly reproduces the temporal and spatial variability in primary production and chl-a observed across the shelf, although considerable improvements can be achieved through tuning of key model parameters (work in progress)." (lines 395-398). In the case of the East China and Yellow Seas, we likewise modified some appropriate text, "Discrepancies between the model and observations in this region may be improved by accounting for higher turbidity in relatively shallow water and model refinements related to photo-physiology." (lines 605-607).

1   **S2P3-R (v1.0): a framework for efficient regional modelling of physical and**
2   **biological structures and processes in shelf seas**

3

4   **Robert Marsh[1] Anna E. Hickman[1], and Jonathan Sharples[2,3]**

5

6   [1] University of Southampton, National Oceanography Centre, Southampton UK

7   [2] School of Environmental Sciences, University of Liverpool, Liverpool L69 3BX,
8   United Kingdom

9   [3] National Oceanography Centre, Liverpool, Joseph Proudman Building, 6 Brownlow
10   Street, Liverpool L3 5DA, UK

11

12   **Abstract**

13   An established 1-dimensional model of Shelf Sea Physics and Primary Production
14   (S2P3) is adapted for flexible use in selected regional settings over selected periods of
15   time. This Regional adaptation of S2P3, the S2P3-R framework (v1.0), can be
16   efficiently used to investigate physical and biological phenomena in shelf seas that are
17   strongly controlled by vertical processes. These include spring blooms that follow the
18   onset of stratification, tidal mixing fronts that seasonally develop at boundaries
19   between mixed and stratified water, and sub-surface chlorophyll maxima that persist
20   throughout summer. While not representing 3-D processes, S2P3-R reveals the
21   horizontal variation of the key 1-D (vertical) processes. S2P3-R should therefore only
22   be used in regions where horizontal processes - including mean flows, eddy fluxes
23   and internal tides - are known to exert a weak influence in comparison with vertical
24   processes. In such cases, S2P3-R may be used as a highly versatile research tool,
25   alongside more complex and computationally expensive models. In undergraduate
26   oceanography modules and research projects, the model serves as an effective
27   practical tool for linking theory and field observations. Three different regional
28   configurations of S2P3-R are described, illustrating a range of diagnostics, evaluated
29   where practical with observations. The model can be forced with daily meteorological
30   variables for any selected year in the reanalysis era (1948 onwards). Example

simulations illustrate the considerable extent of synoptic-to-interannual variability in the physics and biology of shelf seas. In discussion, the present limitations of S2P3-R are emphasised, and future developments are outlined.

1. Introduction

In a global context, the shelf seas are disproportionately productive due to the continuous supply of nutrients (Holt et al., 2009a, and references therein). A variety of models have been developed to explore the processes that shape and maintain productivity. Operational biogeochemistry and ecosystem models typically represent the system with relatively high complexity and resolution, e.g., the 7 km Atlantic Margin Model NEMO-ERSEM (AMM7-NE) system (Edwards et al., 2012) – see also http://www.metoffice.gov.uk/research/news/marine-predictions. Such models may perform well alongside observations, but simulations rely on high performance computing resources such that extensive experimental work is consequently not practical.

In contrast to complex models, the Shelf Sea Physics and Primary Production (S2P3) model (Simpson and Sharples, 2012) exploits the dominance of vertical processes over horizontal processes in shelf seas. S2P3 explicitly represents vertical heat fluxes, vertical mixing of momentum, and vertical mixing of heat and tracers (nitrate and chl-a concentrations). Central to the model physics is a turbulence closure scheme, determining the light environment and nutrient fluxes that drive a simple primary production (nutrient-phytoplankton, or NP) model. Phytoplankton growth responds to changes in stratification and mixing. In this way, S2P3 can efficiently simulate the seasonal cycle of stratification and primary production at a selected location, characterized by a local depth and tidal current amplitude. In particular, S2P3 has been used (e.g., Sharples, 2008) to simulate idealized seasonal tidal mixing fronts (TMFs), analogous to the observed discontinuities between mixed and seasonally stratified water in mid-latitude shelf seas (Simpson and Hunter, 1974). While controlled to first order by vertical processes, the transition from mixed to stratified water across a TMF typically occurs on a horizontal scale of ~10-20 km (e.g., Moore et al., 2003), so for clear resolution of associated physical and biogeochemical structures, TMFs are ideally simulated at high horizontal resolution (1-2 km).

63 S2P3 was introduced as PHYTO-1D and originally described in Sharples (1999). An

64 updated version of PHYTO-1D was described in Sharples (2008). The model is

65 designed for use as an investigative (and educational) tool (see zipped material at

66 http://pcwww.liv.ac.uk/~jons/model.htm). S2P3 has been used as a research tool to

67 establish the varying influence of winds and air-sea heat fluxes on inter-annual

68 variability in the timing of stratification and the spring bloom in the northwestern

69 North Sea (Sharples et al., 2006), and to quantify the impact of spring-neap tidal

70 cycles on biological productivity at TMFs (Sharples, 2008). In educational contexts,

71 S2P3 and forerunner models have been used for around 10 years in Year 3

72 undergraduate and masters-level postgraduate teaching at the Universities of

73 Southampton and Liverpool, in the UK.

74 In spite of potential for widespread application, S2P3 has not been extensively used

75 and tested across real transects or in limited regions, where the model can be

76 appropriately used for investigating time-evolving stratification and biological

77 productivity. Introduced here, S2P3-R is a framework for using S2P3 to efficiently

78 model physical and biological structures in shelf seas, for selected years during the

79 reanalysis era (Kalnay et al., 1996). The development of S2P3-R has facilitated the

80 simulation of vertical processes and their horizontal variability in real-time, for quick

81 investigation of ongoing changes and detailed fieldwork planning.

82 In the remainder of the paper, we first outline the S2P3-R framework. We start with a

83 brief description of the physical and biological components of S2P3, followed by

84 details of the modified source code, model performance and diagnostic options. This

85 is in turn followed by details on model setup in different domains (horizontal meshes

86 and tidal forcing), and the specification of meteorological forcing. We then evaluate

87 model simulations for four different regions, undertaken and diagnosed using the new

88 framework. In discussion, some important caveats are emphasised, and we outline the

89 prospects for development of the S2P3-R framework.

90

91 **2. The S2P3-R framework**

92 *2.1 S2P3*

93   Here, we provide a brief description of the physical and biological components of

94   S2P3, emphasizing key equations. For a more detailed model description, the reader is

95   referred to Sharples (1999) and Sharples (2008).

96

97   *2.1.1 Physical model*

98   Central to the physics of S2P3 is a turbulence closure scheme, for which the

99   prognostic variable is turbulent kinetic energy (TKE), formally defined as $q^2/2$, where

100   q is the turbulent intensity, or velocity scale (m s^{-1}). For a tidal current with x- and y-

101   components u and v, the tendency of TKE is expressed as

102

103
$$\frac{\partial}{\partial t}\left(\frac{q^2}{2}\right) = \frac{\partial}{\partial z}\left(K_q \frac{\partial}{\partial z}\left(\frac{q^2}{2}\right)\right) + N_z\left[\left(\frac{\partial u}{\partial z}\right)^2 + \left(\frac{\partial v}{\partial z}\right)^2\right] + K_z\left(\frac{g}{\rho}\frac{\partial \rho}{\partial z}\right) - \frac{q^3}{B_1 l}$$
$$(1)$$

104

105   where ρ is density, quadratic in temperature T (ρ = 1028.11 - 6.24956 × 10^{-2}T -

106   5.29468 × 10^{-3}T^2, assuming a constant salinity of 35.00), B_1 is a constant of the

107   closure scheme, K_q is the vertical eddy diffusivity for TKE, K_z is the vertical eddy

108   diffusivity for other scalar properties, N_z is vertical eddy viscosity, and l is an eddy

109   length-scale [l = $\kappa z(1 - z/h)^{0.5}$, at depth z, given total depth h and von Karmen's

110   constant κ = 0.41]. Forward time stepping is explicit throughout, with time-steps, Δt,

111   constrained by the diffusive stability criterion, $\Delta t < \Delta z^2/2N_z$, given depth intervals, Δz.

112

113   Tides and winds force the TKE profile for given boundary conditions:

114

115
$$q^2_{z=h} = B_1^{2/3}\frac{\tau_s}{\rho_{z=h}} \;;\quad q^2_{z=0} = B_1^{2/3}\frac{\tau_b}{\rho_{z=0}}$$
$$(2a,b)$$

116

117   where τ_s is the surface ($z = h$) stress due to the wind, and τ_b is the near-bottom ($z = 0$)

118   stress due to tidal currents. The x- and y-components of wind stress are obtained as

119

120
$$\tau_{sx} = -c_d\rho_a u_w\sqrt{(u_w^2 + v_w^2)}; \quad \tau_{sy} = -c_d\rho_a v_w\sqrt{(u_w^2 + v_w^2)}$$ (3a,b)

121

122 given a drag coefficient c_d [$c_d = (0.75 + 0.067w) \times 10^{-3}$, for wind speed w], air density

123 ρ_a (= 1.3 kg m^{-3}), and u_w and v_w, the x- and y-components of wind. The x- and y-

124 components of near-bottom stress are obtained as

125

126
$$\tau_{bx} = -k_b\rho_0 u_1\sqrt{(u_1^2 + v_1^2)}; \quad \tau_{by} = -k_b\rho_0 v_1\sqrt{(u_1^2 + v_1^2)}$$ (4a,b)

127

128 given a drag coefficient k_b (= 0.003), representative density for seawater ρ_0 (= 1025

129 kg m^{-3}), and u_1 and v_1, the x- and y-components of the current 1m above the seabed.

130 See Sharples (1999) for further details on the subsequent calculation of K_z, K_q and N_z.

131 In addition to mixing, the water column is locally heated and cooled. The tendency of

132 temperature (T) is obtained at each depth level as

133

134
$$\frac{\partial T}{\partial t} = \frac{\partial}{\partial z}\left(K_z\frac{\partial T}{\partial z}\right) + Q_h(z)$$ (5)

135

136 where z is height above the seabed and $Q_h(z)$ is the net heating at depth z.

137 Heat fluxes are formulated as follows. We first define a surface net heat flux (Q_{net}) as

138 the sum of incoming shortwave radiation (Q_{SW}), long-wave back radiation (Q_{LW}), and

139 latent and sensible heat exchange with the atmosphere (Q_{sens} and Q_{lat}):

140

141
$$Q_{net} = Q_{SW} - (Q_{LW} + Q_{sens} + Q_{lat})$$ (6)

142

143 Incoming shortwave radiation, irradiance in the presence of clouds, is calculated as

144

145
$$Q_{SW} = (1.0 - 0.004C - 0.000038C^2)Q_{SW,c-s}$$ (7)

146

147 where C is cloud fraction, and clear sky irradiance, $Q_{SW,c\text{-}s}$, is obtained as

148

$$Q_{SW,c-s} = S(1 - \alpha)f(\theta, t)(1 - \kappa_{SW}) \tag{8}$$

150

151 where S is the solar constant (= 1368 Wm^{-2}), α is an atmospheric albedo (= 0.24),
152 $f(\theta,t)$ is a function representing the daily and seasonal variation in day length at
153 latitude θ, and κ_{SW} is a short-wave absorption coefficient (= 0.06). Long-wave
154 radiation is calculated as

155

$$Q_{LW} = \varepsilon_{LW}(1.0 - 0.6{\times}10^{-4}C^2)(0.39 - 0.05q^{0.5})\sigma T^4 \tag{9}$$

157

158 where ε_{LW} is long-wave emissivity (= 0.985), q is vapour pressure ($q = Rq_s$, given
159 saturated vapour pressure $q_s(T)$ and relative humidity R), and σ is the Stefan-
160 Boltzmann constant ($\sigma = 5.67 \times 10^{-8}$ W m^{-2} K^{-4}). Sensible heat flux is calculated using
161 the bulk formula:

162

$$Q_{sens} = \rho_a c_p C_h U(T_s - T_a) \tag{10}$$

164

165 where c_p is the specific heat capacity of air ($c_p = 1004$ J kg^{-1} K^{-1}), C_h is a transfer
166 coefficient ($C_h = 1.45 \times 10^{-3}$), U is surface wind speed, T_s is the sea surface
167 temperature, and T_a is surface air temperature. Latent heat flux is calculated using the
168 bulk formula:

169

$$Q_{lat} = \rho_a L_v C_e U(q_s - q) \tag{11}$$

171

172 where L_v is the specific heat capacity of air ($L_v = 2.5 \times 10^6 - 2.3 \times 10^3 T_s$), and C_e is a
173 transfer coefficient ($C_e = 1.5 \times 10^{-3}$).

174 The surface net heat flux is partitioned down the water column as follows. The red
175 end of the spectrum, 55% of shortwave radiation, is assumed to be absorbed at the top
176 depth level, hence the surface heating, $Q_{h,0} = 0.55Q_{SW} - (Q_{LW} + Q_{sens} + Q_{lat})$. The
177 remaining 45% of insolation is available for heating at lower levels, distributed
178 exponentially throughout the water column as a heating rate $Q_h(z)$, according to

179

180
$$\frac{\partial Q_h}{\partial z} = -Q_h(z)\big(\lambda_0 + \varepsilon X_T(z)\big) \tag{12}$$

181

182 where λ_0 is an attenuation coefficient ($\lambda_0 = 0.1$ m^{-1}) and ε is a pigment absorption
183 cross-section ($\varepsilon = 0.012$ m^2 (mg chl)$^{-1}$), accounting for shading due to $X_T(z)$, the local
184 chlorophyll-a (chl-a) concentration (mg chl m^{-3}), taking $X_T(z) = q^{chl}P_C$, for cell chl-
185 a:carbon ratio, q^{chl} (0.03 mg chl (mg C)$^{-1}$), and carbon concentration, P_C (see below).
186

187 *2.1.2 Biological model*

188 Phytoplankton is modelled in terms of an equivalent carbon concentration (P_C, units
189 mg C m^{-3}) and internal cellular nitrogen (P_N). In each grid cell, P_C tendency is due to
190 the net effect of vertical mixing, growth and grazing, according to

191

192
$$\frac{\partial P_C}{\partial t} = \frac{\partial}{\partial z}\Big(K_z \frac{\partial P_C}{\partial z}\Big) + \mu P_C - G P_C \tag{13}$$

193

194 given a grazing impact rate G, and a growth rate, μ, that is a function of
195 photosynthetically-active radiation:

196

197
$$\mu = \mu_m\big(1 - e^{-(\alpha I_{PAR}\theta/\mu_m)}\big) - r^B \tag{14}$$

198

199 where α is the maximum quantum yield, I_{PAR} is the light availability, θ is the chl-
200 a:carbon ratio, r^B is the respiration rate, and the maximum growth rate, μ_m, is given by

201

$$\mu_m = 1.16{\times}10^{-5} \left(\frac{Q-Q_{sub}}{Q_m-Q_{sub}}\right) 0.59e^{0.0633T} \tag{15}$$

where $Q = P_N/P_C$ is the cell nitrogen quota, Q_{sub} is the subsistence nutrient:carbon quota, and Q_m is the maximum cell quota. The tendency for phytoplankton nitrogen (P_N) is similarly described as

$$\frac{\partial P_N}{\partial t} = \frac{\partial}{\partial z}\left(K_z \frac{\partial P_N}{\partial z}\right) + uP_C - GP_N \tag{16}$$

where the uptake rate u is obtained as a Michaelis-Menton function of the dissolved inorganic nitrogen concentration (DIN):

$$u = \left[u_m \left(1 - \frac{Q}{Q_m}\right)\frac{DIN}{(k_u+DIN)}\right] + \begin{cases} \mu Q \, , \mu < 0 \\ 0 \quad , \mu \geq 0 \end{cases} \tag{17}$$

given k_u, a half saturation coefficient for nutrient uptake, and u_m, a maximum nutrient uptake rate. The uptake of nitrogen leads to a tendency in dissolved inorganic nitrogen (DIN):

$$\frac{\partial DIN}{\partial t} = \frac{\partial}{\partial z}\left(K_z \frac{\partial DIN}{\partial z}\right) - \mu P_C + eGP_N \tag{18}$$

where e is the fraction of grazed phytoplankton cellular nitrogen recycled immediately back into the dissolved nitrogen pool.

Water column nitrogen is constantly restored towards an initial winter concentration, DIN_0 (mmol m^{-3}), by a flux of inorganic nitrogen from the seabed:

$$\frac{\partial DIN_1}{\partial t} = \frac{f_{DIN}}{\Delta z}\left(1 - \frac{DIN_1}{DIN_0}\right) \tag{19}$$

8

229 where DIN_1 is the dissolved nitrogen in the bottom depth cell of the model grid, Δz

230 (m) is the thickness of the model grid cell, and f_{DIN} (mmol m^{-2} s^{-1}) is the maximum

231 flux of dissolved nitrogen from the seabed into the bottom depth cell.

232

233 The values of biological parameters (G, μ_m, θ, r^B, Q_{sub}, α, u_m, Q_m, k_u, e, DIN_0, f_{DIN}) are

234 as listed in Table I of Sharples (2008).

235

236 *2.2 Modified S2P3 source code, performance and diagnostics*

237 For the S2P3-R framework, we modified the Fortran 90 source code of S2P3 v7.0,

238 which includes additional commands and subroutines to facilitate the Winteracter

239 Fortran GUI toolset (Interactive Software Services Ltd., www.winteracter.com), the

240 model being supplied with a text book (Simpson and Sharples, 2012) as an executable

241 application that runs under the Windows operating system. This source code was

242 modified for compilation and execution in a Unix environment by removing GUI-

243 related lines of code. These changes are solely to facilitate compilation and execution

244 in Unix environments, and S2P3 is thus far unchanged as a scientific tool.

245 Within the new framework, S2P3 can be used to generate geographically specific

246 maps, sections and time series, with varying run-time implications on a single

247 processor. Maps typically comprise 5000-20000 grid-points, while sections comprise

248 10-100 grid-points. For a given year (see below), maps can take over a day to

249 generate (depending on the extent of shallower water, where shorter time-steps are

250 necessary), while sections typically take a few minutes, and annual time series at a

251 single location typically take a few seconds.

252 Default mapped variables are the mid-summer surface-bottom temperature difference,

253 annual-mean surface heat flux, and annual net production. Other quantities, such as

254 the mid-summer sub-surface chl-a maximum (SCM) and SCM depth, can also be

255 mapped. The option for simulating sections is motivated by opportunities for direct

256 comparison with measurements obtained through surveys and cruises. In selecting to

257 simulate section data, constant depth intervals are specified for plotting on a regular

258 distance-depth mesh without the need for interpolation. The option for time series at

259 single locations is motivated by the availability of time series at repeat Conductivity

260 Temperature Depth (CTD) stations and moorings. Finally, we save daily horizontal

261   distributions of physical and biological variables for selected periods, to generate

262   animations that yield a range of insights not so easily appreciated with individual

263   maps or sections.

264   FORTRAN programmes are used to post-process model data for plotting, and

265   MATLAB scripts are used to plot model variables (as used to prepare the figures and

266   animations presented here). Example MATLAB plotting scripts are provided together

267   with the source code and other ancillary programmes and data files in s2p3-reg.zip

268   (see "Code availability").

269

270   *2.3 Regional configurations*

271   Three domains have been developed and tested here, for reasons that are outlined in

272   turn. Figure 1 shows the bathymetry, while Table 1 specifies the boundaries,

273   resolution, tidal forcing and initial temperature field, for each domain. In an initial

274   stage of development, S2P3-R was developed for the northwest European shelf

275   domain. Development of the two other domains has been motivated by the extent to

276   which the different climatological and tidal forcing can be accommodated (in the shelf

277   seas around China) and by ongoing fieldwork (annual surveys south of Cornwall) in a

278   smaller region where the tidal mixing front is particularly sharp.

279   Bathymetry is typically in the range 50-100 m across most of the northwest European

280   shelf (Fig. 1a). However, some important details are emphasised for the other two

281   domains: a shallower inshore zone (depths < 30 m) in the Western English Channel

282   (Fig. 1b); a secondary shelf break (descending 50-100 m) in the East China Sea (Fig.

283   1c). At very high resolution, some artefacts of bathymetric surveying are apparent as

284   linear features in the bathymetry south of Cornwall (Fig. 1b).

285   For the northwest European shelf, bathymetry and current amplitudes for the leading

286   three tidal constituents (M2, S2, N2 - see Fig. S1 in Supplementary Material) were

287   obtained from the POLCOMS model (e.g., Holt et al., 2009b). For the Western

288   English Channel, bathymetry is extracted from the ETOPO1 global relief model

289   (Amante and Eakins, 2009) and tidal current amplitudes are interpolated from the

290   POLCOMS dataset. For the East China and Yellow Seas, current amplitudes for the

291   leading 13 tidal constituents were generated using OTPS (OSU Tidal Prediction

292   Software), based on the inverse method developed by Egbert et al. (1994) and Egbert

293 and Erofeeva (2002), and bathymetry is selected within the OTPS system. Opting to

294 use the leading five constituents for this region, S2P3 was adapted to include the two

295 diurnal constituents, O1 and K1, in addition to the semi-diurnal constituents S2, M2

296 and N2 (see Fig. S2).

297 One further distinction in regional setup concerns initial temperatures. At 1 January of

298 each year, the water column across the European shelf seas is presumed mixed

299 everywhere. In the default model, initial temperature is 10.1°C at all depths,

300 appropriate for the Celtic Sea. This initial temperature is also appropriate for the

301 Western English Channel, although we specify simulated 31 December temperatures

302 (constant through the fully mixed water column) for subsequent 1 January dates in the

303 case of simulations at the Western Channel Observatory (see Section 3.2). Elsewhere,

304 alternative values for initial temperature are appropriate, consistent with local climate.

305 Consider as an example the northeast sub-region of our northwest European shelf

306 domain. Sensitivity tests illustrate the importance of specifying an appropriate initial

307 temperature − see Fig. S3. If the initial temperature in this region is too high (Fig.

308 S3a), the net heat fluxes fall below -10 Wm^{-2} across much of the domain, especially to

309 the north (i.e., annual net cooling from a "warm start"), while if the temperature is too

310 low (Fig. S3b), heat fluxes exceed 10 Wm^{-2} at most locations (i.e., annual net

311 warming from a "cold start"). Only if the initial temperature is accurate to within

312 around 1°C do we avoid strong annual net cooling or heating (Fig. S3c). For the

313 China Seas, we specify a higher initial temperature of 15.1°C and simulate two

314 consecutive years, accounting for weak wintertime stratification in this region. We

315 analyse only the second year, for which more realistic initial conditions are thus

316 established across the wider domain (on 1 January of the second year).

317

318 *2.4 Meteorological forcing*

319 In addition to tidal mixing, S2P3 is forced with surface heat fluxes and wind stirring.

320 Heat is gained by shortwave radiation and lost via long-wave back-radiation, sensible

321 and latent heat fluxes - see Eqn. (6). Shortwave radiation varies with latitude and time

322 of year, and decreases with fractional cloud cover - see Eqns. (7) and (8). Long-wave

323 radiation varies with sea surface temperature and cloud cover – see Eqn. (9). Sensible

324   and latent heat losses vary with air temperature, wind speed and relative humidity

325   according to bulk formulae – see Eqns. (10) and (11).

326   Daily values for the four necessary meteorological variables are provided in a single

327   ASCII file. Sharples (2008) uses climatological meteorological data for the Celtic

328   Sea, while Sharples et al. (2006) use meteorological data for 1974-2003 from weather

329   stations in the vicinity of a study site in the northwestern North Sea. Here, we use

330   NCEP Reanalysis data provided by the NOAA/OAR/ESRL PSD, Boulder, Colorado,

331   USA, from their website at http://www.esrl.noaa.gov/psd/. These data are routinely

332   updated to within a day or so of the present time, and span the period from 1948. The

333   data is provided on a 2.5° global mesh, so each domain is forced everywhere with

334   meteorological data from a single 2.5° grid square, central to that region. Coordinates

335   of selected grid squares are listed in Table 1.

336   Figure 2 illustrates time series of meteorological variables for the three domains. In

337   initial testing, for the northwest European shelf, we use the "default" Celtic Sea

338   climatology (Sharples, 2008). For the other two domains, data for 2013 are shown for

339   example. Note the extent of high-frequency synoptic variability in these cases, in

340   particular for relative humidity, cloud fraction and wind speed. Also note that the UK

341   spring of 2013 was exceptionally cold, hence air temperatures for the Western English

342   Channel sub-domain considerably below the Celtic Sea climatological average. Also

343   note considerable contrast between the maritime and continental climates, for the

344   European shelf and China Seas respectively.

345

346   **3. Model evaluation in the new framework**

347   *3.1 Northwest European shelf*

348   Figure 3 shows a summary of fields obtained for a simulation using the northwest

349   European shelf domain. Fig. 3a shows the annual-mean Hunter-Simpson parameter,

350      $\log_{10}(h/u^3)$, where h is the local depth and u is the amplitude of the local tidal current.

351   Previous studies (starting with Simpson and Hunter, 1974) have established a

352   threshold value of around 2.7, below (above) which the water column is well mixed

353   (stratified). $\log_{10}(h/u^3)$ is generally below 2.7 throughout the southern North Sea, and

354   across much of the eastern English Channel and the Irish Sea. These regions are

355   indeed well mixed throughout summer, as evident in near-zero surface-bottom

356   temperature differences for mid-July, shown in Fig. 3b. Elsewhere, stratification is
357   established, and the model hence simulates a set of fronts between mixed and
358   stratified water that are clearly observed in satellite data (see Fig. 8.1 in Simpson and
359   Sharples, 2012 - also indicated in Fig. 3a): the Islay front between Northern Ireland
360   and Scotland (A); the Western Irish Sea front enclosing a seasonally-stratified region
361   of the Irish Sea (B); part of the Cardigan Bay front (C); the St George's Channel front
362   between Wales and Ireland (D); the Ushant and Western English Channel front
363   between southwest England and Brittany, France (E). The model also simulates a
364   front observed between the seasonally-stratified northern North Sea and the
365   permanently mixed southern North Sea, including the Flamborough frontal system
366   (Hill et al., 1993, and references therein), also indicated (F) in Fig. 3a.

367   A limitation of the simulation presented in Fig. 3 is the use of default climatological
368   meteorological forcing, originally set up for simulating tidal mixing fronts in the
369   Celtic Sea. This has important consequences for local heat balances, evaluated here
370   with the annual-mean surface net heat flux, shown in Fig. 3c. In the central Celtic Sea
371   (south of Ireland), the net heat flux is slightly positive, in the range 0-5 Wm^{-2}.
372   Elsewhere, one might expect that a warmer (cooler) sea surface will lead to stronger
373   net heat loss (gain), via sensible and latent heat fluxes. However, the imbalance
374   reaches a maximum of 10 Wm^{-2} in the warm southwest English Channel (net heating)
375   and a minimum of -10 Wm^{-2} in the cool northern North Sea (net cooling). This is
376   consistent with insolation levels at these latitudes that are respectively higher and
377   lower than that for the Celtic Sea. Such imbalances are also a consequence of
378   specifying the same initial temperature everywhere (see section 2.2), such that the
379   northern North Sea is initially too warm (so must lose heat over the seasonal cycle),
380   and the southwest English Channel is initially too cool (so must gain heat). Net heat
381   fluxes are also notably positive in some regions that are well mixed all year round, in
382   particular the Irish Sea and parts of the English Channel. This is consistent with
383   enhanced heat storage due to mixing throughout the water column of heat gained in
384   summer (Simpson and Bowers, 1984).

385   We have also experimented, on the northwest European shelf domain, with spatially
386   discriminate initial temperatures and meteorological forcing (not shown here), the
387   latter respecting variation of NCEP reanalysis data (per 2.5° grid square) across the
388   domain. While this approach has the potential to restrict net heat fluxes closer to zero

13

at all locations, coarse-resolution data must be carefully interpolated to the relatively

390 fine 12-km mesh of S2P3-R in order to avoid unrealistic horizontal variations in

391 forcing and simulated fields.

392 Depending on temperature and the co-availability of photosynthetically active

393 radiation (PAR) and nutrients, the model simulates primary production. Annual net

394 carbon production per unit area is shown in Fig. 3d and simulated surface chl-a is

395 compared to satellite observations in Fig S4 and S5. The model broadly reproduces

396 the temporal and spatial variability in primary production and chl-a observed across

397 the shelf, although considerable improvements can be achieved through tuning of key

398 model parameters (work in progress).

399 Surface production rates (Fig 3d) and chl-a concentrations (Fig. S4) are especially

400 high in shallow coastal water that remains well mixed for most/all of the year, where

401 nutrients are consequently continuously re-supplied from the seabed, and PAR levels

402 are sufficient at all depths to maintain photosynthesis. We have limited confidence in

403 the simulated primary production and chl-a close to the coasts, for two specific

404 reasons. We do not account for the strong influence near many coasts of freshwater

405 (runoff), which has an important stratifying influence on the water column. We also

406 neglect the higher turbidity caused by non-algal particles that can reduce PAR below

407 a level necessary to sustain photosynthesis, e.g., where sediment loads are relatively

408 high in shallow regions of vigorous mixing, such as the southern North Sea.

409 Recognizing this model limitation, we choose not to plot model output in water

410 shallower than 30 m in Figs. 3 and S4.

411 Moving towards stratified regions, annual-mean carbon production rates generally

412 decline, although remain above 55 g C m^{-2} year^{-1} at most locations due to the

413 combined result of the major spring and minor autumn blooms (see below). This

414 decline is complemented by elevated productivity throughout summer at the

415 thermocline, associated with the development and persistence of the sub-surface chl-a

416 maximum (SCM). Primary production rates during the spring bloom (not shown)

417 reach 40 g C m^{-2} mon^{-1} or 1333 mg C m^{-2} d^{-1}, in line with observed magnitudes in the

418 order of 1000 mg C m^{-3} d^{-1} (Rees et al., 1999). Summertime chl-a and primary

419 production are low in the surface mixed layer, consistent with observed values of <1

420 mg chl-a m^{-3} and 5-30 mg C m^{-3} d^{-1}, respectively (Joint et al., 2000; Hickman et al.,

421 2009). Simulated surface chl-a concentrations are broadly consistent with satellite

422 observations, although values are typically double those observed (see Figs. S4 and
423 S5). The model does not reproduce the enhanced primary production and chl-a
424 observed in the surface at the Celtic Sea shelf break (e.g., compare Figs. S4 and S5,
425 for April and May). This is likely because it does not include specific physical
426 processes, such as the internal tide, that are important for vertical nutrient supply to
427 the surface in these regions (Sharples et al., 2007).

428 Following the spring bloom, surface productivity and surface chl-a concentrations
429 remain elevated (above background values) near three tidal mixing fronts in particular
430 – the Ushant and Western English Channel front, the Islay front, and the St George's
431 Channel front – for June-September in the simulation (Fig. S4) and for May-July in
432 the observations (Fig. S5). Surface chl-a concentrations decline towards more
433 stratified waters, coincident with deepening of the SCM away from fronts and
434 associated zones of spring-neap frontal adjustment (Pingree et al., 1978; Weston et al.,
435 2005; Hickman et al., 2012). At the Ushant Front, predicted peak July primary
436 production of 80-100 mg C m^{-3} d^{-1} is considerably smaller than in situ measurements
437 of 59-126 mg C m^{-3} h^{-1} (implying daily production of around 1000 mg m^{-3} d^{-1}), for
438 surface waters at a frontal station in late July (Holligan et al., 1984). However, the
439 model estimates are intermediate between corresponding surface observations for
440 mixed and stratified waters (reported in Holligan et al., 1984), emphasizing the very
441 localized character of frontal productivity, which is not easily captured with our
442 relatively coarse model resolution (here around 12 km) and in the absence of
443 horizontal processes that may lead to convergence of material at the front.

444 In the southern Irish Sea and south of the Islay front, simulated surface chl-a
445 concentrations are notably very low, at around 0.1 mg chl-a m^{-3} (see Fig. S4). These
446 low values are found in regions where the tidal current amplitude is especially strong
447 (see Fig. S1) in water that is sufficiently deep (~100 m, see Fig. 1a) for PAR to fall
448 below a threshold value within the well-mixed water column (Fig. 3b). So in spite of
449 very high nutrient levels throughout the year (not shown), light is a severe limitation
450 on photosynthesis and hence productivity. This aspect of the simulation is inconsistent
451 with surface chl-a concentrations of around 1 mg chl-a m^{-3} observed in this region
452 (Fig. S5; Pemberton et al., 2004; Moore et al., 2006). A likely explanation is that the
453 model does not resolve photo-acclimation, the known ability of phytoplankton to
454 acclimate to ambient light conditions (e.g., Geider et al., 1997), and so does not

15

455 resolve the photo-physiological differences between stratified and mixed water

456 columns (Moore et al., 2006). Dissolved inorganic nitrate (DIN) concentrations in the

457 northwest European shelf region during winter and in the bottom mixed layer during

458 summer (not shown) are 5-6 mmol m^{-3}, consistent with observed values around 6-9

459 mmol m^{-3} (Joint et al., 2001; Hickman et al., 2012).

460 To illustrate typical vertical structure across a mid-summer tidal mixing front, Figure

461 4 shows observations and corresponding simulations for day 215 (3 August) of 2003,

462 along a section through the Celtic Sea front (Fig. 4a), located at around 52°N. The

463 temperature distribution (Fig. 4b,c) illustrates stratified water south of 52°N, with

464 mixed water to the north. DIN concentrations are high in mixed water and in the

465 lower layer of the stratified water, and depleted in the surface layer of the stratified

466 water (Fig. 4d,e). Chl-a concentrations reach a surface maximum at the front, with

467 elevated values extending southwards in the model - the SCM supported by a weak

468 diffusive DIN flux across the thermocline (Fig. 4f,g).

469 Comparing the simulation with the observations, the mixed water is about 1°C cooler

470 than observed, and DIN and chl-a concentrations are about 50% higher at most

471 depths. Regarding structural discrepancy between observed chl-a concentrations in

472 Fig. 4f and modeled chl-a concentrations in Fig. 4g, the northward-shifted surface

473 maximum in the model is coincident with a more northward location of the tidal

474 mixing front, which could be attributed to inadequacies in meteorological and/or tidal

475 forcing. The higher surface maximum of chl-a in the model may be in part due to

476 neglected horizontal processes, such as along-front transports by a baroclinic jet

477 supported by strong horizontal temperature gradients, and cross-frontal mixing

478 processes associated with jet instability. Higher chl-a concentrations in the model may

479 alternatively be attributed to the relatively simple description of phytoplankton

480 physiology, grazing and mobility (no sinking, as default).

481

482 *3.2 Western English Channel*

483 For 1 May to 7 October of 2013, selected daily model fields are saved and animated

484 (see Supplementary Material Part B, "Example Animation", and accompanying

485 commentary text). A wide range of phenomena are evident in the animation, including

486 the earliest establishment of stratification during May, expressed as a surface-bottom

temperature difference, and the rapid uptake of surface DIN, which declines to near-zero concentrations with the development of a spring bloom (high surface chl-a levels) that peaks in early-mid June. We note that the exceptionally cold spring of 2013 substantially delayed the onset of stratification and the spring bloom (also suggested by satellite data – not shown). The spring-neap cycle of stronger mixing (on spring tides) and strengthened stratification (on neap tides) causes ~14-day "beating" of chl-a concentration, between low values on spring tides and high values on neap tides, most notably at the front between inshore mixed and offshore stratified waters off southwest Cornwall throughout June and July.

To illustrate the interannual variability of summer stratification, Figure 5 shows surface-bottom temperature differences on day 190 (8 or 9 July) of 2002-13. The region is characterized by mixed water to the northwest associated with locally strong tidal current amplitudes (see Fig. S1), and stratified water to the southwest (where tides are weaker), with a secondary area of stratification centred around 4.5° W 50.1° N (coincident with a local minimum in tidal current amplitude). The water column remains mixed all year round in shallow water close to the coast, at most locations and in most years. A complex arrangement of mixed and stratified water is simulated in the northeast of the region, associated with highly variable bathymetry (see Fig. 1b). When a cold spring is followed by a warm summer (e.g., 2006, 2010, 2013), stratification is particularly strong, with surface-bottom temperature differences reaching almost 7°C in the southwest of the region.

To locally validate the simulation, we use observations at L4 (50° 15.00' N, 4° 13.02' W) and E1 (50° 02.00' N, 4° 22.00' W), hydrographic stations that have been occupied weekly and monthly, respectively, as part of the Western Channel Observatory (http://www.westernchannelobservatory.org.uk/data.php). Here, seasonal cycles of stratification and phytoplankton dynamics have been extensively studied (Smyth et al. 2010). In Fig. 5, we over-plot observed temperature differences for station occupations within a few days (L4) or 1-2 weeks (E1) of day 190. Observed differences are generally indistinguishable from the simulated differences.

For a more comprehensive validation, Figure 6 shows time series of surface-bottom temperature differences observed and (daily) simulated at L4 and E1. The temperature at the depth of the maximum chl-a concentration is also plotted at E1, confirming the existence of an SCM within the seasonal thermocline. Starting on 1 January 2002, we

520   simulate one year at a time, specifying a mixed water column temperature on, e.g., 1

521   January 2003 with the corresponding temperature on 31 December 2002, etc. This

522   ensures continuity in temperatures between years, respecting a small degree of

523   interannual variability in wintertime temperature at L4 and E1. Weak stratification

524   (maximum ~4°C) typically is established over ~5 months of each summer at L4,

525   while stronger stratification (up to ~7°C) develops for longer (by 1-2 months) at E1.

526   Model-observation agreement is remarkably good, with close correspondence

527   between not just surface temperatures, but also bottom temperatures. The seasonally

528   varying stratification at both stations is generally reproduced to within 1°C, although

529   high-frequency extremes are under-sampled by weekly (monthly) occupations of L4

530   (E1), and there is more disagreement at L4. This is most likely because the water

531   column at L4 is strongly influenced by freshwater, with low surface salinity having a

532   substantial effect on stratification. The vertical salinity distribution also explains the

533   apparent temperature instability (negative surface-bottom temperature differences)

534   observed at L4 in winter - the water column is in fact statically stable throughout the

535   time series.

536   With some confidence in model performance, in Figure 7 we show temperature, DIN

537   and chl-a in sections through the developing tidal mixing front east of Lizard

538   peninsula, along 50.017°N, on days 100, 130, 160 and 190 of 2013. We select this

539   section as representative of CTD transects undertaken annually in late June/early July

540   by University of Southampton fieldwork students. On day 100 (early April), the water

541   column is well mixed almost everywhere, with very weak stratification in temperature

542   evident at 10 km along the section. DIN concentrations are high (~6 mmol m^{-3})

543   throughout the water column for bottom depths exceeding a threshold value (~40 m),

544   below which PAR falls below a critical value within the water column. As bottom

545   depths become shallower (progressing inshore), DIN concentrations rapidly fall to

546   near zero, where PAR is sufficient at all depths to sustain plankton growth and

547   associated DIN uptake in the model. Inshore chl-a concentrations are accordingly high

548   (12-13 mg chl-a m^{-3}), falling rapidly with distance to background values (~0.1 mg

549   chl-a m^{-3}) offshore.

550   By day 130 (early May), the water remains well mixed, although warmer by 1-2°C,

551   and high productivity has spread offshore, presumably due to intermittent weak

552   stratification during preceding days. By day 160, stratification is clearly established

553   beyond 4 km offshore. DIN concentrations are now reduced to near-zero in the upper

554   20 m of the stratified water, and high chl-a concentrations are evidence of the spring

555   bloom. By day 190, stratification has strengthened and DIN concentrations in the deep

556   layer of stratified water columns are further depleted through vertical mixing with the

557   upper photic zone, although surface chl-a concentrations have by this time

558   substantially declined in the upper layer. The boundary between mixed and stratified

559   waters on days 160 and 190 marks the position of the tidal mixing front. The model

560   has been further used to evaluate the extent of interannual variability around the time

561   of annual fieldwork, in the third week of June. Temperature sections on day 169 of

562   2002-13 (see Figure S6) reveal a wide range of offshore stratification and frontal

563   structure in recent years, with strongest stratification in 2010, weakest stratification in

564   2011, and a most clearly defined front in 2009.

565   As an example of the seasonal cycles in temperature, surface DIN and surface chl-a at

566   four locations across the front (spanning the distance range 3-7 km in Fig. S6), Figure

567   8 shows evolution of these variables through 2013. Stratification is very marginal and

568   intermittent at 5.033°W, with surface-bottom temperature differences occasionally

569   reaching 2°C. DIN concentrations fall close to zero over days 130-300 and chl-a

570   concentrations are high (in the range 6-8 mg chl-a m^{-3} throughout this period. Related

571   to the intermittent stratification are similar fluctuations in chl-a. This variability is in

572   part attributed to the near-fortnightly spring-neap tidal cycle, which leads to periodic

573   replenishment of nutrients, out of phase with more favourable PAR regimes.

574   Progressing offshore into deeper water, the seasonal cycle transforms towards

575   stronger stratification, a shorter period of surface DIN reduction, and a stronger peak

576   in surface chl-a around day 150 that corresponds to the spring bloom, followed by

577   substantially lower concentrations during the rest of summer.

578

579   *3.3 East China and Yellow Seas*

580   Figure 9 shows example fields for a simulation using the East China Sea and Yellow

581   Sea domain with 2013 forcing. Fig. 9a shows the annual-mean Hunter-Simpson

582   parameter, $\log_{10}(h/u^3)$, which falls below 2.7 in particularly shallow regions (see Fig.

583   1c) that are also characterized by high amplitude tidal currents (see Fig. S2).

584      $\log_{10}(h/u^3)$ conversely exceeds 5.0 in the isolated Bohai Sea, lying to the northwest of

585   the Yellow Sea. As for the northwest European shelf, regions with $\log_{10}(h/u^3) < 2.7$

586   remain well mixed throughout summer (Fig. 9b). Elsewhere, stratification is stronger

587   than for the northwest European shelf, with surface-bottom temperature differences

588   on day 190 of ~10°C across much of the stratified shelf. A major feature of Fig. 9b is

589   the front between mixed and stratified water in the East China Sea that is clearly

590   observed in satellite SST data (Hickox et al., 2000). The simulations also capture the

591   complex system of fronts observed in the Taiwan Strait (Zhu et al., 2013).

592   The specification of common meteorological variables across ~20° of latitude and

593   ~15° of longitude is a considerable approximation, and the annual-mean net surface

594   heat flux field is an important measure of resulting heat imbalances (Fig. 9c). We

595   regard these values as not too excessive, ranging from around 5 Wm^{-2} (heat gain) in

596   the far south to around -10 Wm^{-2} (excess heat loss) in the far north (Bohai Sea).

597   Annual-mean carbon production rates in the well-mixed shallow regions of the East

598   China Sea range from 300 to 450 g C m^{-2} $year^{-1}$, falling to ~100 g C m^{-2} $year^{-1}$ in the

599   more extensive stratified region (Fig. 9d). These predictions are similar in magnitude

600   to estimates of primary production based on in situ observations (e.g., 145 g C m^{-2}

601     $year^{-1}$ for "the entire shelf of the East China Sea", Gong et al. 2003). Monthly-mean

602   surface chl-a distributions are broadly comparable to satellite observations, although

603   maximum model chl-a concentrations are generally double those observed, and the

604   spring bloom is ~1 month late, in May rather than April (e.g., for 2013, Figs. S7 and

605   S8). Discrepancies between the model and observations in this region may be

606   improved by accounting for higher turbidity in relatively shallow water and model

607   refinements related to photo-physiology.

608   To complete the three-dimensional picture, Figure 10 shows show temperature, DIN

609   and chl-a concentration in sections through the developing front of the central East

610   China Sea, along 32°N, on days 100, 130, 160 and 190 of 2013. Bottom depth

611   increases considerably with distance offshore. In water of depth < 40 m, the water

612   column remains well-mixed throughout the year, while in deeper water, stratification

613   becomes established between days 100 and 130. In stratified water, DIN is already

614   depleted in the surface layer over days 100-130, and is gradually further depleted in

615   the lower layer over days 130-190 through progressive mixing into the photic zone. A

616   local surface maximum in chl-a concentration is evident at the frontal boundary (~250

617　km) on day 130, while a SCM is evident in stratified water on days 160 and 190. The

618　SCM is most clearly defined at ~25 m on day 190.

619

620　**4. Summary and discussion**

621　We have developed S2P3-R, a versatile framework for efficient modeling of physical

622　and biological phenomena and processes in shelf seas, adopting an existing 1-D

623　model, S2P3. Here, we complement ongoing development and use of the 1-D model

624　for specific research hypotheses (e.g., Bauer and Waniek, 2013) and in educational

625　settings, where idealized simulations (e.g., Sharples, 2008) are linked to realistic

626　situations such as fieldwork contexts - e.g., off Cornwall, away from the lateral

627　influences of runoff.

628　The realism of S2P3-R depends on the extent to which vertical processes dominate

629　horizontal processes. This is evident across some shelf sea regions, where we have the

630　high-quality observations necessary for a co-evaluation of these processes. One way

631　to formally quantify the dominance of surface net heat fluxes and tidal plus wind

632　mixing (the 1-D processes) is by calculating tendencies of the potential energy

633　anomaly (PEA, see Chapter 6 in Simpson and Sharples, 2012). PEA tendencies

634　calculated directly from observed changes of stratification at selected locations (e.g.,

635　weekly/monthly at Western Channel Observatory stations L4/E1) can be compared

636　with indirect estimates computed from time-integrated heat fluxes, winds and tidal

637　currents at the same locations. If local heat fluxes and tidal/wind mixing dominate the

638　annual cycle of stratification, directly calculated and indirectly estimated time series

639　of PEA tendency should be similar.

640　Where appropriate, the framework facilitates experiments to investigate the sensitivity

641　of measurable quantities (e.g., chl-a concentration) to a wide range of physical and

642　biological processes that can be adjusted with corresponding model parameters.

643　Where high quality observations are available (e.g., at E1 in the western English

644　Channel), S2P3-R thus provides a means for improving our fundamental

645　understanding of the system. With tuned parameters, S2P3-R furthermore provides

646　the means to carry out credible multi-year simulations of physical and biological

647　processes and property distributions at appropriately high temporal, vertical and

648　horizontal resolution.

21

649　At the seasonal timescale, the most striking surface features are tidal mixing fronts

650　(TMFs). Realistic representation of TMFs, demanding high horizontal resolution,

651　amounts to first-order evaluation of any simulation, e.g., the UK Met Office forecast

652　system (O'Dea et al., 2012), which has the same relatively coarse (12 km) resolution

653　as our northwest European shelf domain. The summer surface-bottom temperature

654　differences across the northwest European shelf and the associated TMFs in S2P3-R

655　(Fig. 3a) compare well with the 3-D model results (O'Dea et al., 2012, their Fig. 10).

656　Our simpler approach thus indicates the importance of 1-D processes in forming these

657　features, the locations of which are consistent with these more complex models.

658　It is natural to deploy S2P3 across multiple processors, with sub-domains computed

659　independently in parallel. This has been trialled for twelve $1° \times 1°$ sub-domains across

660　the southern Celtic Sea and western English Channel at a resolution of 1 km,

661　substantially expanding our Western English Channel domain with essentially no

662　extra computational expense. Figure 11 shows the July surface-bed temperature

663　difference across this region, illustrating how we are able to efficiently simulate

664　regional stratification at very high horizontal resolution.

665　We have evaluated the model in various ways with available observations,

666　specifically addressing spatial patterns, vertical structures, and seasonal-interannual

667　variability. Temperature distributions are reproduced with considerable success, as are

668　key aspects of the spatial and temporal variability in nutrient and chl-a concentrations.

669　In particular, we are able to accurately reproduce monthly observations of thermal

670　structure at station E1 in the western English Channel over 2002-13 (Fig. 6),

671　providing confidence in the use of S2P3-R in this region. We therefore consider there

672　is much potential for S2P3-R to investigate physical and physiological controls on

673　primary productivity at regional scales.

674　Elsewhere, differences between the model and observations are informative because,

675　for example, they identify regions in which processes other than those represented in

676　the model are important. In particular, we note several processes specific to coasts and

677　shelf breaks, of relevance to several physical aspects of the domains considered here:

678　　• The coastal zone around Cornwall, typified by station L4, is strongly

679　　　influenced by riverine inputs that promote surface freshening and stratification

680   and alter light attenuation by non-algal particles and dissolved organic matter

681   (Groom et al., 2009; Smyth et al., 2010)

682   • The northern North Sea is strongly influenced by shelf edge exchange that

683   leads to the inflow of relatively warm and salty Atlantic Water (Huthnance et

684   al., 2009)

685   • The Yangtze River and two branches of the Kuro Shio - the Taiwan Current

686   and the Tsushima Warm Current - exert strong influences on stratification and

687   productivity in the East China Sea (e.g., Son et al., 2006).

688 Further development of S2P3-R will formally establish the (presently prototype)

689 option to prescribe spatially variable initial temperatures and meteorological

690 variables, interpolated appropriately to each model mesh. As an additional diagnostic,

691 the thermal wind balance may be used with the simulated density field to infer the

692 residual flows that are associated with TMFs (e.g., Hill et al., 2008), indicating the

693 potential importance of net advection along the fronts.

694 In summary, the S2P3-R framework (v1.0) provides the flexibility to undertake

695 research experiments in finely-resolved realistic domains where 1-D processes

696 dominate, to test hypotheses regarding the sensitivity of 1-D biogeochemical

697 processes to key model parameters, and/or to test the responses to variations of

698 physical forcing on timescales ranging from diurnal to interannual. Combining

699 flexibility with computational efficiency, the S2P3-R framework may further

700 contribute to capacity building in marine monitoring and management for

701 individuals/organisations without the resources to run or analyse complex models of

702 their territorial waters or exclusive economic zones.

703

704 **Code availability**

705 The S2P3-R (v1.0) framework, comprising source code along with example scripts

706 and output, is available online from:

707 `ftp://ftp.noc.soton.ac.uk/pub/rma/s2p3-reg.tar.gz`

708 Unzipped and uncompressed, the directory `/s2p3_reg_v1` contains several sub-

709 directories:

- `/main` contains the source code, `s2p3v7_reg_v1.f90`, which is compiled "stand-alone", and executed using accompanying scripts, with examples of "map" (the northwest European Shelf simulation, as Fig. 3), "section" (Celtic Sea) and "time series" (E1) simulations (`run_map`, `run_section` and `run_timeseries`, respectively)
- `/domain` contains bathymetry and tide data for the northwest European Shelf region (`s12_m2_s2_n2_h_map.asc`), for a selected north-south section in the Celtic Sea (`s12_m2_s2_n2_h_sec.asc`) and for a selected point, E1 in the western English Channel (`s12_m2_s2_n2_h_tim.asc`)
- `/met` contains climatological meteorological forcing (`Celtic_met.dat`)
- `/output` contains example output data from the three runs (map, section, time series)
- `/plotting` contains MATLAB scripts for plotting maps, sections and time series (`plot_map`, `plot_section` and `plot_timeseries`, respectively)

The ancillary files needed for simulations in the domains "Western English Channel" and "East China and Yellow Seas", and for a selection of years, are available on request from the author (e-mail rm12@soton.ac.uk).

741 **References**

742

743 Amante, C. and B. W. Eakins (2009). ETOPO1 1 Arc-Minute Global Relief Model:
744   Procedures, Data Sources and Analysis. NOAA Technical Memorandum
745   NESDIS NGDC-24, 19 pp.

746

747 Bauer, A., and J. J. Waniek (2013). Factors affecting the chlorophyll a concentration
748   in the central Beibu Gulf, South China Sea, *Mar. Ecol. Prog. Ser.*, **474**, 67-88,
749   doi:103354/meps10075

750

751 Edwards, K. P., Barciela, R., and M. Butenschön (2012). Validation of the NEMO-
752   ERSEM operational ecosystem model for the North West European Continental
753   Shelf, *Ocean Sci.*, **8**, 983-1000, doi:10.5194/os-8-983-2012.

754

755 Egbert, G. D., Bennett, A. F., and M. G. G. Foreman (1994). TOPEX/POSEIDON
756   tides estimated using a global inverse model. *J. Geophys. Res.*, **99**, 24821-
757   24852, doi:10.1029/94JC01894

758

759 Egbert, G. D., and S. Y. Erofeeva (2002). Efficient Inverse Modeling of Barotropic
760   Ocean Tides. *J. Atmos. Oceanic Technol.*, **19**, 183–204. doi:
761   http://dx.doi.org/10.1175/1520-0426(2002)019<0183:EIMOBO>2.0.CO;2

762

763 Geider, R. J., MacIntyre, H. L., and T. M. Kana (1997). A dynamic model of
764   phytoplankton growth and acclimation: responses of the balanced growth rate
765   and chlorophyll a:carbon ratio to light, nutrient-limitation and
766   temperature. *Mar. Ecol. Prog. Ser.*, **148**, 187-200.

767

768 Gong, G.-C., Wen, Y.-H., Wang, B.-W., and G.-J. Liu (2003). Seasonal variation of
769   chlorophyll a concentration, primary production and environmental conditions
770   in the subtropical East China Sea. *Deep-Sea Research II*, **50**, 1219–1236,

771

772 Groom, S., Martinez-Vicente, V., Fishwick, J., Tilstone, G., Moore, G., Smyth, T.,
773   and D. Harbour (2009). The Western English Channel Observatory: optical
774   characteristics of station L4. *J. Mar. Sys.*, **77**, 278-295.

775

776   Hickman, A. E., Holligan, P. M., Moore, C. M., Sharples, J., Krivtsov, V. and M. R.

777   Palmer (2009). Distribution and chromatic adaptation of phytoplankton within a

778   shelf sea thermocline. *Limnol. Oceanogr.*, **54**, 525-536.

779

780   Hickman, A. E., Moore, C. M., Sharples, J., Lucas, M. I., Tilstone, G. H., Krivtsov, V.

781   and P. M. Holligan (2012). Primary production and nitrate uptake within the

782   seasonal thermocline of a stratified shelf sea. *Mar. Ecol. Prog. Ser.*, **463**, 39-57,

783   doi:10.3354/meps09836

784

785   Hickox R., I. Belkin, P. Cornillon and Z. Shan (2000). Climatology and Seasonal

786   Variability of Ocean Fronts in the East China, Yellow and Bohai Seas from

787   Satellite SST Data. *Geophy.* Res. Lett., **27**, 2945-2948.

788

789   Hill, A. E., James, I. D., Linden, P. F., Matthews, J. P., Prandle, D., Simpson, J. H.,

790   Gmitrowicz, E. M., Smeed, D. A., Lwiza, K. M. M., Durazo, R., Fox, A. D., and

791   D. G. Bowers (1993). Dynamics of tidal mixing fronts in the North Sea [and

792   discussion]. *Phil. Trans. Roy. Soc. Lond. (A)*, **343**, 1669 (1993): 431-446.

793

794   Hill, A. E., J. Brown, L. Fernand, J. Holt, K. J. Horsburgh, R. Proctor, R. Raine, and

795   W. R. Turrell (2008). Thermohaline circulation of shallow tidal seas. *Geophys.*

796   *Res. Lett.*, **35**, L11605, doi:10.1029/2008GL033459.

797

798   Holligan P. M., Williams, P. J. L., Purdie, D., and R. P. Harris (1984) Photosynthesis,

799   respiration and nitrogen supply of plankton populations in stratified, frontal and

800   tidally mixed shelf waters. *Mar. Ecol. Prog. Ser.*, **17**, 201–213.

801

802   Holt, J., Harle, J., Proctor, R., Michel, S., Ashworth, M., Batstone, C., Allen, I.,

803   Holmes, R., Smyth, T., Haines, K., Bretherton, D., and G. Smith (2009).

804   Modelling the global coastal ocean. *Phil. Trans. Roy. Soc. A*, **367**, 939-951, doi:

805   10.1098/rsta.2008.0210

806

807   Holt, J., Wakelin, S., and J. Huthnance (2009). Down-welling circulation of the

808   northwest European continental shelf:,A driving mechanism for the continental

809   shelf carbon pump. *Geophys. Res. Lett.*, **36**, L14602,
810   doi:10.1029/2009GL038997

811

812 Huthnance, J. M., Holt, J. T., and S. L.Wakelin (2009). Deep ocean exchange with
813   west-European shelf seas. *Ocean Sci.*, **5**, 621–634, www.ocean-
814   sci.net/5/621/2009/

815

816 Joint, I., and S. B. Groom (2000). Estimation of phytoplankton production from
817   space: current status and future potential of satellite remote sensing. *J. Exp.*
818   *Mar. Biol. Ecol.*, **250**, 233-255.

819

820 Kalnay, E., Kanamitsu. M., and R. Kistler (1996). The NCEP/NCAR 40-year
821   reanalysis project, *Bull. Amer. Meteor. Soc.*, **77**, 437-470.

822

823 Moore, C. M., Suggett, D. J., Hickman, A. E., Kim, Y. N., Tweddle, J. F., Sharples,
824   J., Geider, R. J. and P. M. Holligan (2006). Phytoplankton photoacclimation and
825   photoadaptation in response to environmental gradients in a shelf sea. *Limnol.*
826   *Oceanogr.*, **51**, 936-949.

827

828 Moore, C. M., Suggett, D., Holligan, P. M., Sharples, J., Abraham, E. R., Lucas, M.
829   I., Rippeth, T. P., Fisher, N. R., Simpson, J. H., and D. J. Hydes (2003).
830   Physical controls on phytoplankton physiology and production at a shelf sea
831   front: a fast repetition-rate fluorometer based field study *Mar. Ecol. Prog. Ser.*,
832   **259**, 29–45.

833

834 O'Dea, E. J., Arnold, A. K., Edwards, K. P., Furner, R., Hyder, P., Martin, M. J.,
835   Siddom, J. R., Storkey, D., While, J., Holt, J. T., and H. Liu (2012). An
836   operational ocean forecast system incorporating NEMO and SST data
837   assimilation for the tidally driven European North-West shelf. *Journal of*
838   *Operational Oceanography*, 5 (1). 3-17.

839

840 Pemberton, K., Rees, A. P., Miller, P. I., Raine, R., and I. Joint (2004). The influence
841   of water body characteristics on phytoplankton diversity and production in the
842   Celtic Sea. *Cont. Shelf Res.*, **24**, 2011–2028.

843

844 Pingree, R., Holligan, P., and G. T. Mardell (1978). The effects of vertical stability on
845   phytoplankton distributions in the summer on the northwest European Shelf.
846   *Deep Sea Res.*, **25**, 1011–1028.

847

848 Rees, A. P., Joint, I., and K. M. Donald (1999). Early spring bloom phytoplankton-
849   nutrient dynamics at the Celtic Sea Shelf Edge. *Deep Sea Research II*, **46**, 483–
850   510.

851

852 Sharples, J., (1999). Investigating the seasonal vertical structure of phytoplankton in
853   shelf seas. *Marine Models Online.* **1**, 3-38.

854

855 Sharples, J., Ross O.N., Scott, B.E., Greenstreet, S., Fraser, H. (2006). Inter-annual
856   variability in the timing of stratification and the spring bloom in the North-
857   western North Sea. *Cont. Shelf Res.*, **26**, 733-751.

858

859 Sharples, J., Tweddle, J. F., Green, J. A. M., Palmer, M. R., Kim, Y.-N., Hickman, A.
860   E., Holligan, P. M., Moore, C. M., Rippeth, T. P., Simpson, J. H., and V.
861   Krivtsov (2007). Spring-neap modulation of internal tide mixing and vertical
862   nitrate fluxes at a shelf edge in summer. *Limnol. Oceanogr.*, 52, 1735-1747.

863

864 Sharples, J. (2008). Potential impacts of the spring-neap tidal cycle on shelf sea
865   primary production. *Journal of Plankton Research*, **30**, 183-197.

866

867 Simpson, J. H., and J. R. Hunter (1974). Fronts in the Irish Sea. *Nature*, **250**, 404-406.

868

869 Simpson, J. H., and D. G. Bowers (1984). Geographical variations in the seasonal
870   heating cycle in northwest European shelf seas. *Annales Geophysicae*, **2**(4),
871   411-416.

872

873 Simpson, J. H., and J. Sharples (2012). *Introduction to the Physical and Biological*
874   *Oceanography of Shelf Seas*. Cambridge University Press.

875

876 Smyth, T. J., Fishwick, J. R., Al-Moosawi, L., Cummings, D. G., Harris, C., Kitidis,

877   V., Rees, A., Martinez-Vicente, V., and E. M. S. Woodward (2010). A broad

878   spatio-temporal view of the Western English Channel observatory. *J. Plankton*

879   *Res.,* **32**, 585-601. doi: 10.1093/plankt/fbp128

880

881 Son, S., Yoo, S., and J.-H. Noh (2006). Spring phytoplankton bloom in the fronts of

882   the East China Sea. *Ocean Sci. J.*, **41**, 181-189. doi:10.1007/BF03022423

883

884 Weston, K., Fernand, L., Mills, D., Delahunty, R., and J. Brown (2005). Primary

885   production in the deep chlorophyll maximum of the central North Sea. *J*

886   *Plankton Res*, **27**, 909–922.

887

888 Zhu, J., Hu, J., and Z. Liu (2013). On summer stratification and tidal mixing in the

889   Taiwan Strait, *Frontiers of Earth Science*, **7**, 141-150, doi:10.1007/s11707-013-

890   0355-1.

891 **Figure Captions**

892

893 Figure 1. Bottom depth (relative to sea surface) in the three S2P3-R domains: (a)

894 northwest European shelf; (b) western English Channel; (c) East China and Yellow

895 Seas.

896

897 Figure 2. Daily meteorological data: climatological for the northwest European shelf

898 (Sharples, 2008), and for 2013 in the Western English Channel, and in the East China

899 and Yellow Seas: (a) air temperature; (b) wind speed; (c) cloud fraction; (d) relative

900 humidity.

901

902 Figure 3. For the northwest European shelf domain: (a) Hunter-Simpson parameter,

903 highlighting the contour delineating $\log_{10}(h/u^3) = 2.7$; (b) day 190 surface-bottom

904 temperature difference; (c) net surface heat flux; (d) annual net production. In (a), we

905 label fronts as in Fig. 8.1 of Simpson and Sharples (2012): the Islay front (A); the

906 Western Irish Sea front (B); the Cardigan Bay front (C); the St. Georges Channel

907 front (D); the Ushant and Western English Channel front (E). We additionally label

908 the Flamborough frontal system (F).

909

910 Figure 4. Sections through the Celtic Sea front around day 215 of 2003: (a) locations

911 of CTD stations (dots) and model grid-points (circles); (b), (c) observed and modelled

912 temperature (°C); (d), (e) observed and modeled dissolved inorganic nitrate (units

913 mmol m^{-3}); (f), (g) observed and modelled chl-a concentration (units mg chl-a m^{-3}).

914 The locations of observations in profile are indicated by dots in (b), (d) and (f).

915

916 Figure 5. Surface–bottom temperature differences (°C) in the Western English

917 Channel, on day 190 of 2002-13. Coloured circles indicate the coincident temperature

918 differences at L4 and E1, subject to data availability (E1 data are unavailable in 2004,

919 2006 and 2013).

920

921 Figure 6. Time series of surface-bottom temperature differences observed and (daily)

922 simulated at L4 and E1 (http://www.westernchannelobservatory.org.uk/data.php).

923

924   Figure 7. Sections through the developing tidal mixing front east of Lizard peninsula,

925   along 50.017°N, on days 100, 130, 160 and 190 of 2013: temperature (left column);

926   dissolved inorganic nitrate (mmol m^{-3}, middle column); chl-a (mg chl-a m^{-3}, right

927   column).

928

929   Figure 8. Time series of surface and bottom temperature (red and blue curves),

930   surface-bottom temperature difference, surface DIN and surface chl-a concentrations,

931   across the tidal mixing front east of the Lizard peninsula in 2013.

932

933   Figure 9. For the East China and Yellow Seas domain in 2013: (a) Hunter-Simpson

934   parameter, highlighting the contour delineating $\log_{10}(h/u^3) = 2.7$; (b) day 190 surface-

935   bottom temperature difference; (c) net surface heat flux; (d) annual net production.

936

937   Figure 10. Sections through the developing tidal mixing front of the East China Sea,

938   along 32°N, on days 100, 130, 160 and 190 of 2013: temperature (left column); DIN

939   (mmol m^{-3}, middle column); chl-a (mg chl-a m^{-3}, right column).

940

941   Figure 11. Surface-bottom temperature differences (°C) across the southern Celtic Sea

942   and western English Channel, in mid July of 2014, simulated with S2P3-R configured

943   in twelve 1° x 1° sub-domains, as indicated.

944   Table 1. Boundaries, resolution, tidal forcing, initial temperature and meteorological

945   forcing for each domain (POLCOMS = Proudman Oceanographic Laboratory Coastal

946   Ocean Modelling System; OTPS = OSU Tidal Prediction Software)

947

Domain	Boundaries	Resolution	Tidal Forcing	Initial temperature field	Meteorological forcing
northwest European shelf	14.917°W – 1.917°E 48.056°N – 61.944°N	0.167° (longitude) 0.111° (latitude) (~12 km)	M2, S2, N2 (POLCOMS)	10.1°C everywhere (default)	Daily climatology for the Celtic Sea (Sharples, 2008)
Western English Channel	4 – 6°W 49.5 – 50.5°N	1' x 1' (~1 km)	M2, S2, N2 (POLCOMS interpolated)	10.1°C everywhere	Daily NCEP reanalysis data for grid square centred on 5°W, 50°N
East China and Yellow Seas	112 – 130°E 21 – 42°N	0.083° x 0.083° (~6 km)	M2, S2, N2, O1, K1 (OTPS)	After 1-year started from 15.1°C everywhere	Daily NCEP reanalysis data for grid square centred on 125°E, 32.5°N

948
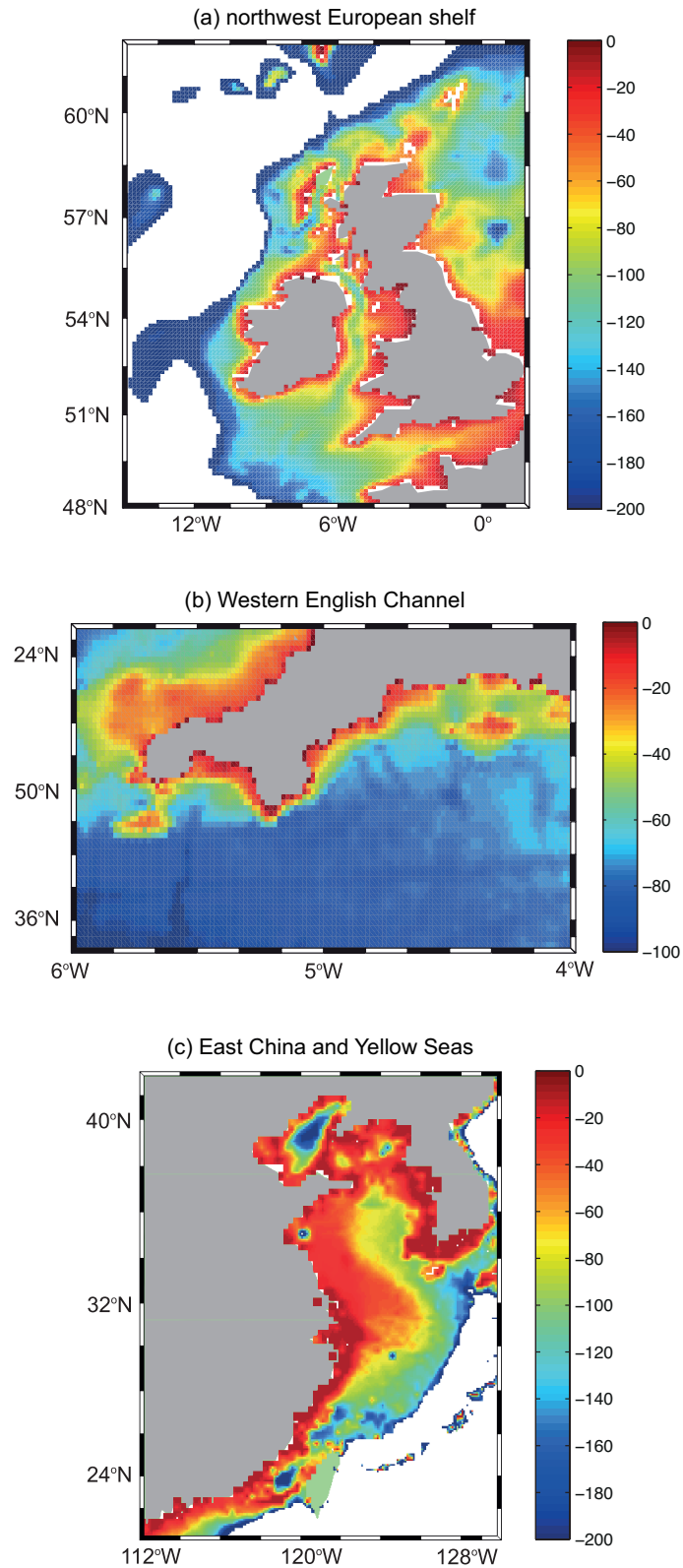
Figure 1. Bottom depth (relative to sea surface) in the three S2P3-R domains: (a) northwest European shelf; (b) western English Channel; (c) East China and Yellow Seas.
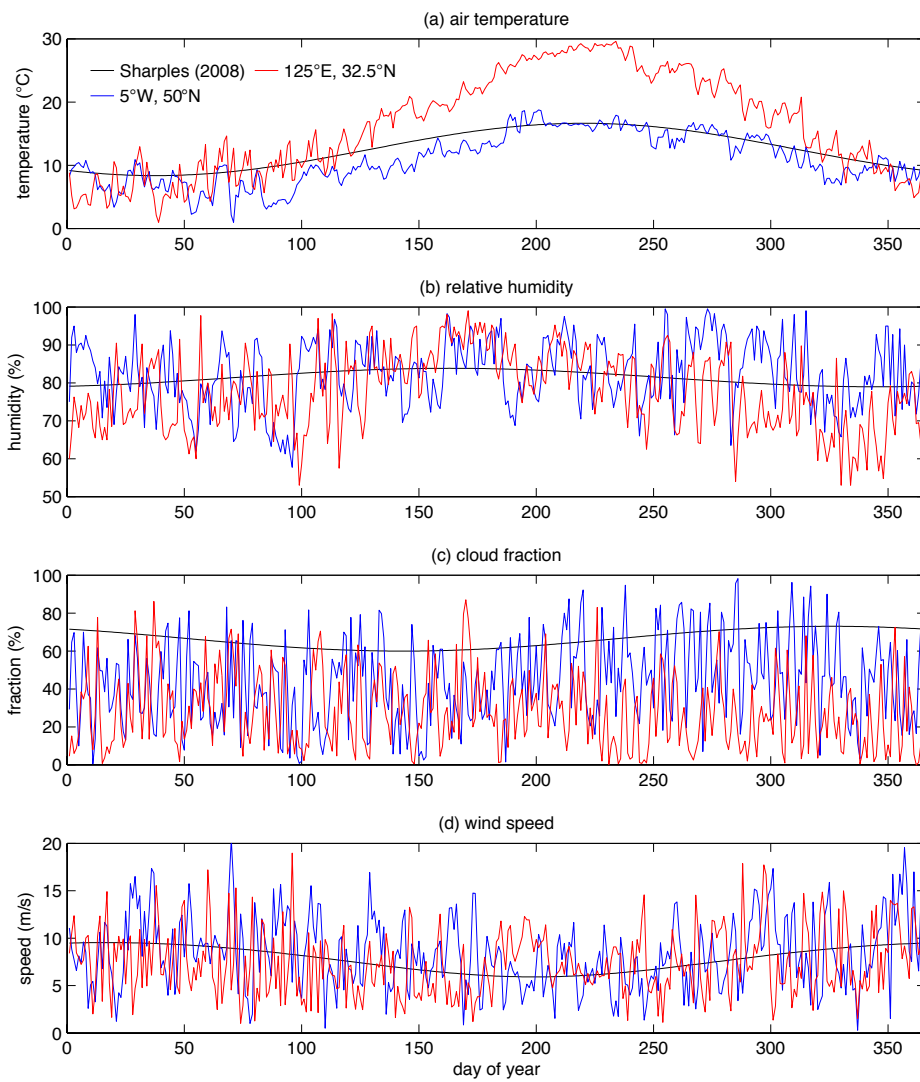
954

955 Figure 2. Daily meteorological data: climatological for the northwest European shelf

956 (Sharples, 2008), and for 2013 in the Western English Channel, and in the East China

957 and Yellow Seas: (a) air temperature; (b) wind speed; (c) cloud fraction; (d) relative

958 humidity.

959

960

961

Figure 3. For the northwest European shelf domain: (a) Hunter-Simpson parameter, highlighting the contour delineating $\log_{10}(h/u^3) = 2.7$; (b) day 190 surface-bottom temperature difference; (c) net surface heat flux; (d) annual net production. In (a), we label fronts as in Fig. 8.1 of Simpson and Sharples (2012): the Islay front (A); the Western Irish Sea front (B); the Cardigan Bay front (C); the St. Georges Channel front (D); the Ushant and Western English Channel front (E). We additionally label the Flamborough frontal system (F).

(a) CTD stations (dots) and model gridpoints (circles)

(b) observed temperature

(c) model temperature

(d) observed nitrate

(e) model nitrate

(f) observed chlorophyll

(g) model chlorophyll

969

970   Figure 4. Sections through the Celtic Sea front around day 215 of 2003: (a) locations

971   of CTD stations (dots) and model grid-points (circles); (b), (c) observed and modelled

972   temperature (°C); (d), (e) observed and modeled dissolved inorganic nitrate (units

973   mmol m^{-3}); (f), (g) observed and modelled chl-a concentration (units mg chl-a m^{-3}).

974   The locations of observations in profile are indicated by dots in (b), (d) and (f).
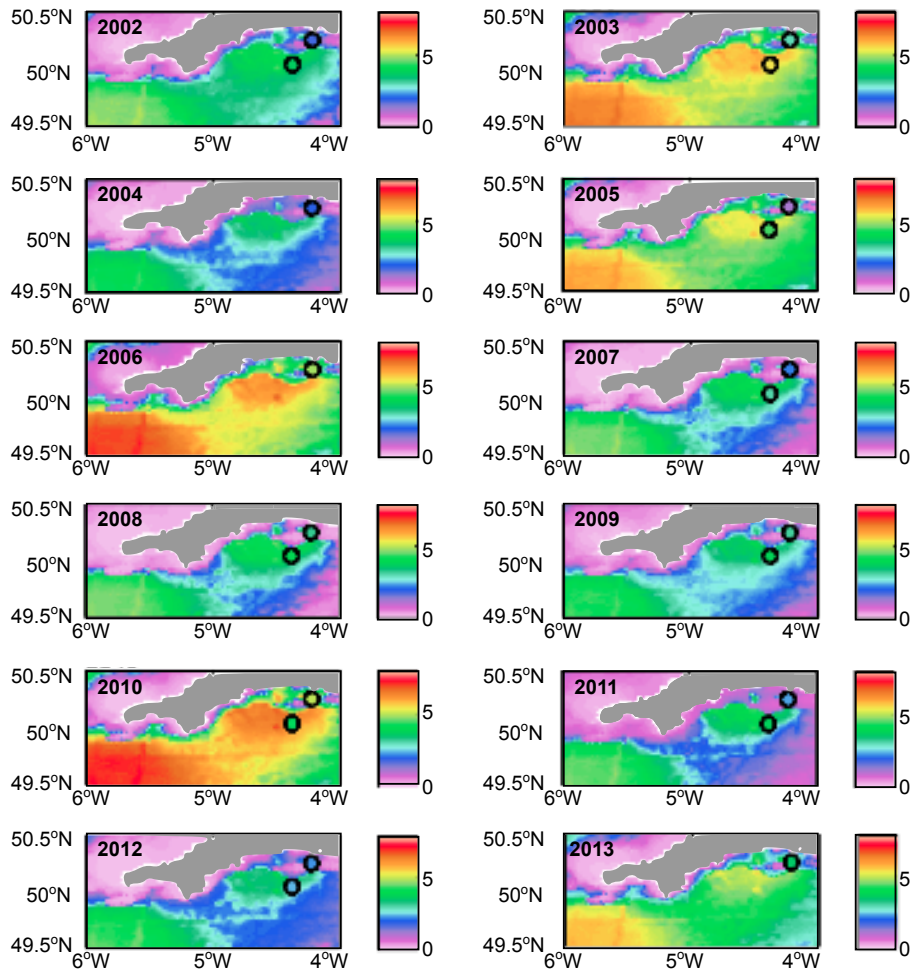
975

976

Figure 5. Surface–bottom temperature differences (°C) in the Western English
Channel, on day 190 of 2002-13. Coloured circles indicate the coincident temperature
differences at L4 and E1, subject to data availability (E1 data are unavailable in 2004,
2006 and 2013).
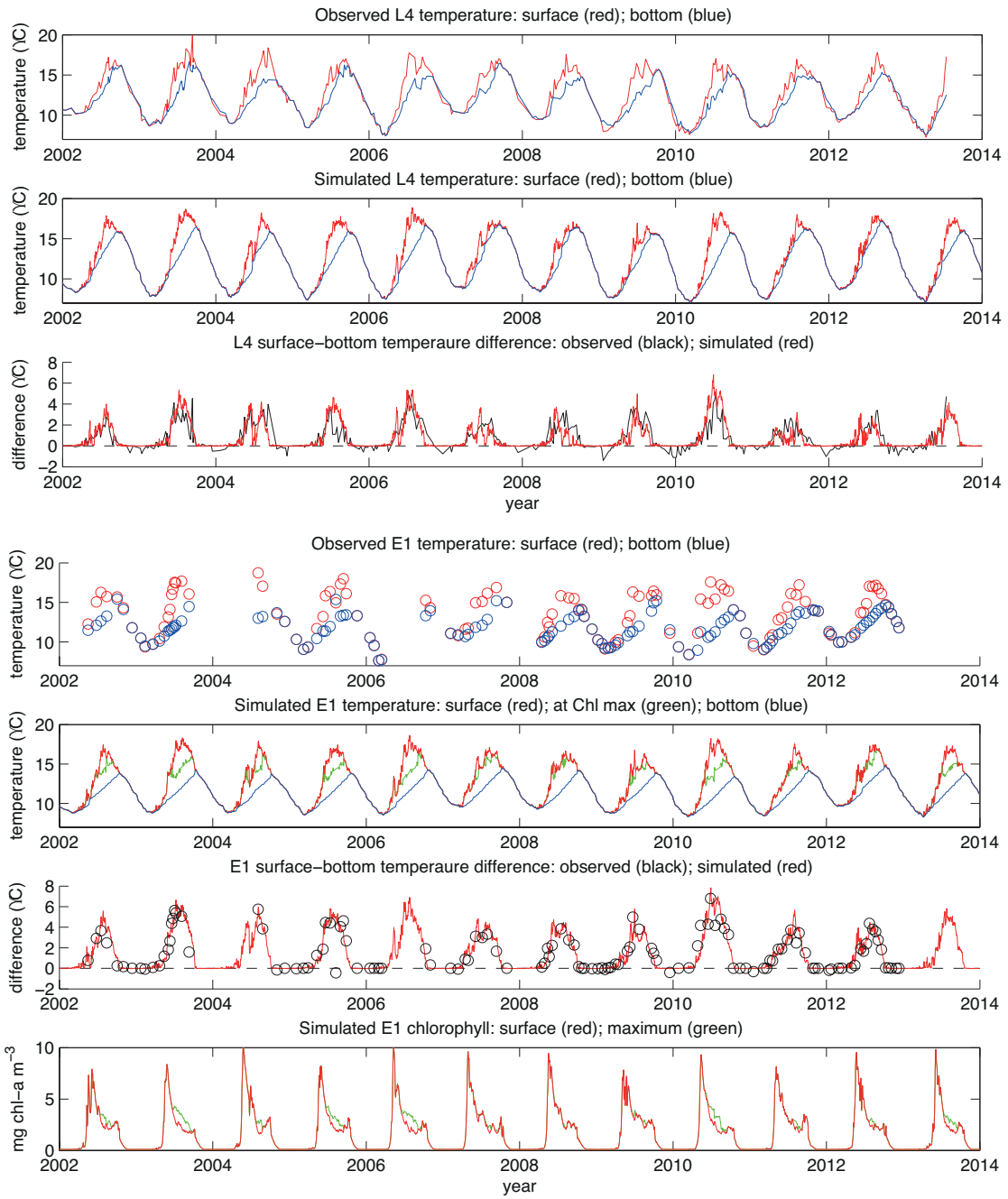
981

982
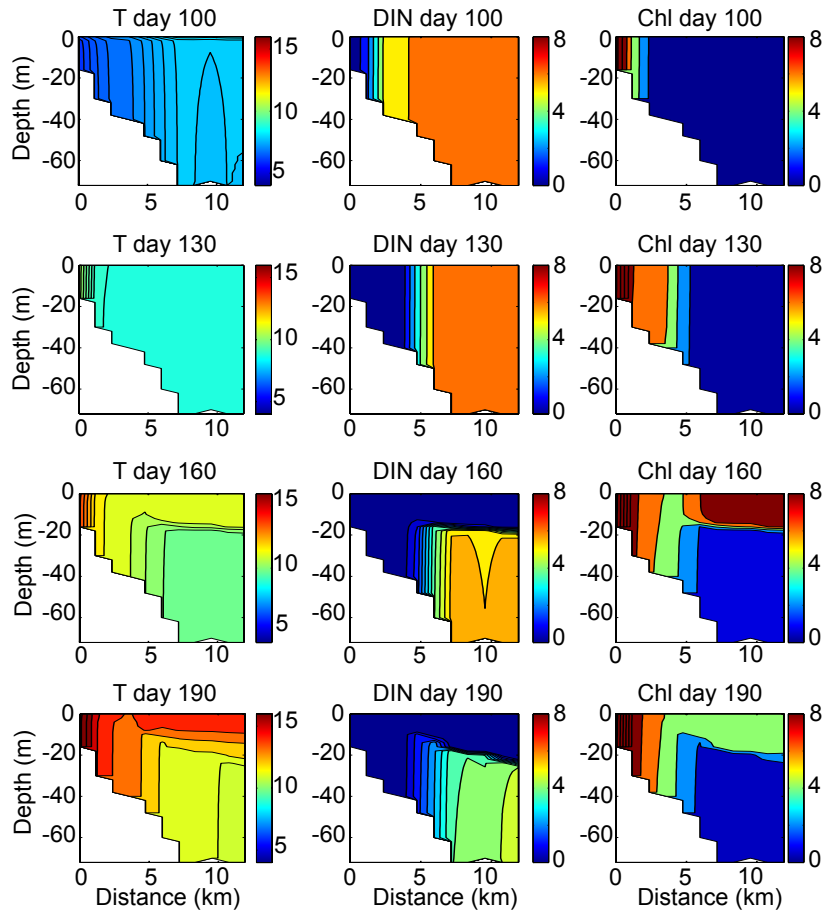
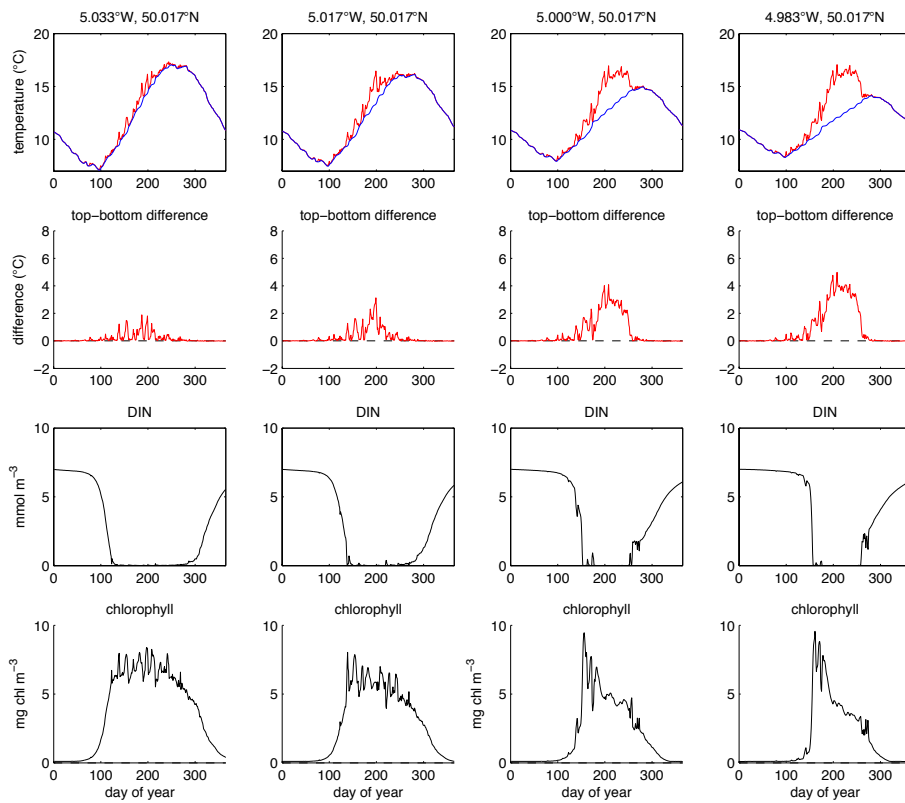983   Figure 6. Time series of surface-bottom temperature differences observed and (daily)

984   simulated at L4 and E1 (http://www.westernchannelobservatory.org.uk/data.php).

Figure 7. Sections through the developing tidal mixing front east of Lizard peninsula, along 50.017°N, on days 100, 130, 160 and 190 of 2013: temperature (left column); dissolved inorganic nitrate (mmol m^{-3}, middle column); chl-a (mg chl-a m^{-3}, right column).

991

992 Figure 8. Time series of surface and bottom temperature (red and blue curves),

993 surface-bottom temperature difference, surface DIN and surface chl-a concentrations,

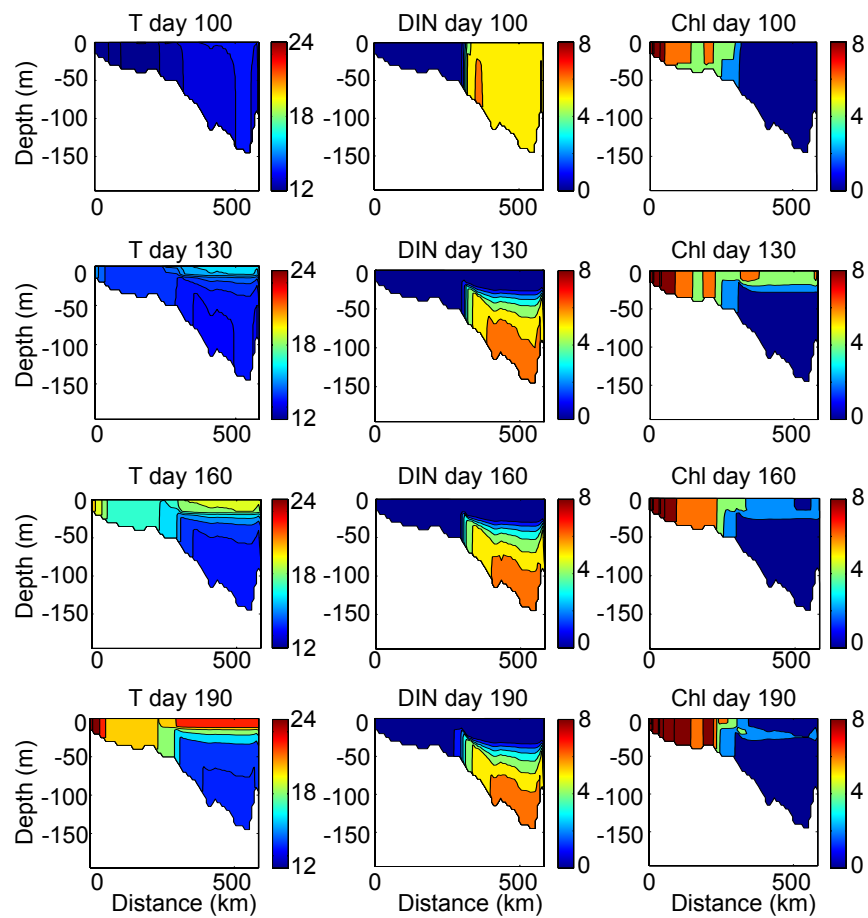994 across the tidal mixing front east of the Lizard peninsula in 2013.
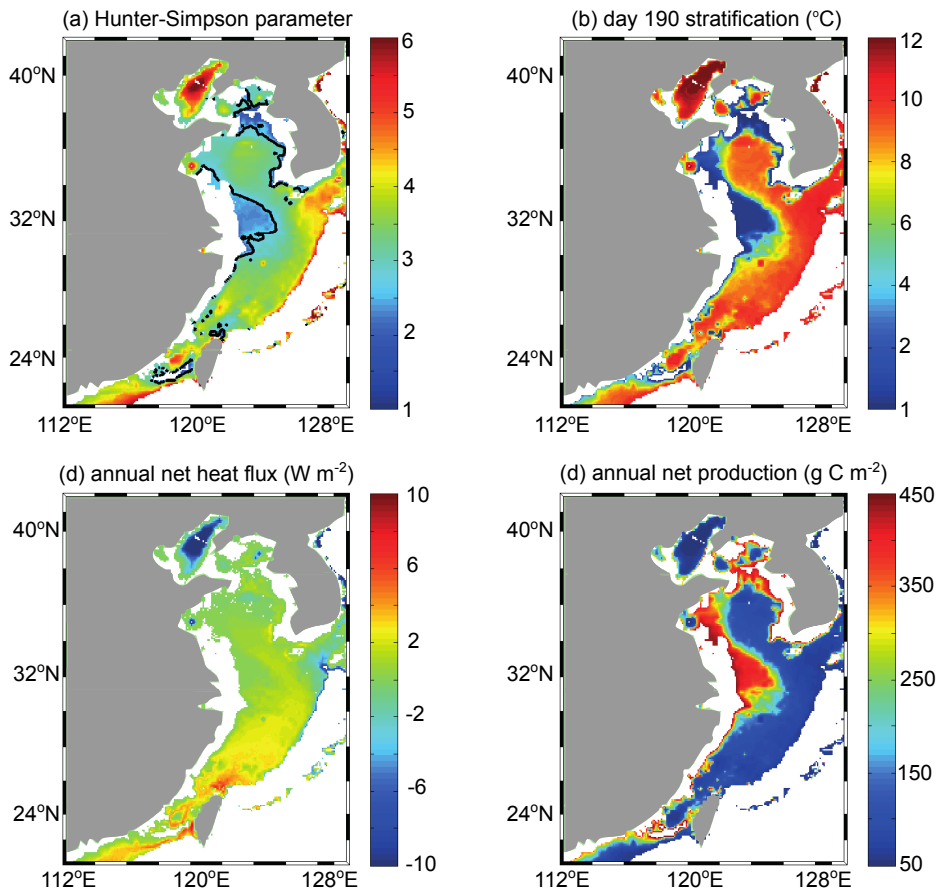
Figure 9. For the East China and Yellow Seas domain in 2013: (a) Hunter-Simpson parameter, highlighting the contour delineating $\log_{10}(h/u^3) = 2.7$; (b) day 190 surface-bottom temperature difference; (c) net surface heat flux; (d) annual net production.
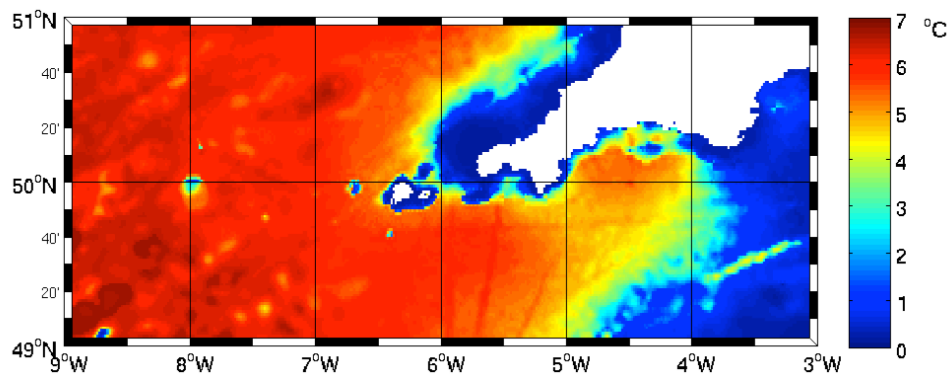
1000

1001

1002

1003 Figure 10. Sections through the developing tidal mixing front of the East China Sea,

1004 along 32°N, on days 100, 130, 160 and 190 of 2013: temperature (left column); DIN

1005 (mmol m^{-3}, middle column); chl-a (mg chl-a m^{-3}, right column).

1006

1007

1008

1009   Figure 11. Surface-bottom temperature differences (°C) across the southern Celtic Sea

1010   and western English Channel, in mid July of 2014, simulated with S2P3-R configured

1011   in twelve 1° x 1° sub-domains, as indicated.